

# PCCP

Accepted Manuscript



This is an *Accepted Manuscript*, which has been through the Royal Society of Chemistry peer review process and has been accepted for publication.

*Accepted Manuscripts* are published online shortly after acceptance, before technical editing, formatting and proof reading. Using this free service, authors can make their results available to the community, in citable form, before we publish the edited article. We will replace this *Accepted Manuscript* with the edited and formatted *Advance Article* as soon as it is available.

You can find more information about *Accepted Manuscripts* in the [Information for Authors](#).

Please note that technical editing may introduce minor changes to the text and/or graphics, which may alter content. The journal's standard [Terms & Conditions](#) and the [Ethical guidelines](#) still apply. In no event shall the Royal Society of Chemistry be held responsible for any errors or omissions in this *Accepted Manuscript* or any consequences arising from the use of any information it contains.

## Molecular Characterization of Brown Carbon (BrC) Chromophores in Secondary Organic Aerosol Generated From Photo-Oxidation of Toluene

Peng Lin,<sup>a</sup> Jiumeng Liu,<sup>b</sup> John E Shilling,<sup>b</sup> Shawn M. Kathmann,<sup>c</sup> Julia Laskin,<sup>c</sup> Alexander Laskin<sup>a,\*</sup>

<sup>a</sup>*Environmental Molecular Sciences Laboratory, Pacific Northwest National Laboratory, Richland, WA*

<sup>b</sup>*Atmospheric Sciences & Global Change Division, Pacific Northwest National Laboratory, Richland, WA*

<sup>c</sup>*Physical Sciences Division, Pacific Northwest National Laboratory, Richland, WA*

\* corresponding author

Revised manuscript submitted to

PCCP

June 2, 2015

**ABSTRACT**

Atmospheric Brown carbon (BrC) is a significant contributor to light absorption and climate forcing. However, little is known about a fundamental relationship between the chemical composition of BrC and its optical properties. In this work, light-absorbing secondary organic aerosol (SOA) was generated in the PNNL chamber from toluene photo-oxidation in the presence of NO<sub>x</sub> (Tol-SOA). Molecular structures of BrC components were examined using nanospray desorption electrospray ionization (nano-DESI) and liquid chromatography (LC) combined with UV/Vis spectroscopy and electrospray ionization (ESI) high-resolution mass spectrometry (HRMS). The chemical composition of BrC chromophores and the light absorption properties of toluene SOA (Tol-SOA) depend strongly on the initial NO<sub>x</sub> concentration. Specifically, Tol-SOA generated under high-NO<sub>x</sub> conditions (defined here as initial NO<sub>x</sub>/toluene of 5/1) appears yellow and mass absorption coefficient of the bulk sample ( $MAC_{\text{bulk}}@365\text{nm} = 0.78 \text{ m}^2 \text{ g}^{-1}$ ) is nearly 80 fold higher than that measured for the Tol-SOA sample generated under low-NO<sub>x</sub> conditions (NO<sub>x</sub>/toluene < 1/300). Fifteen compounds, most of which are nitrophenols, are identified as major BrC chromophores responsible for the enhanced light absorption of Tol-SOA material produced in the presence of NO<sub>x</sub>. The integrated absorbance of these fifteen chromophores accounts for 40-60% of the total light absorbance by Tol-SOA at wavelengths between 300 nm and 500 nm. The combination of tandem LC-UV/Vis-ESI/HRMS measurements provides an analytical platform for predictive understanding of light absorption properties by BrC and their relationship to the structure of individual chromophores. General trends in the UV/vis absorption by plausible isomers of the BrC chromophores were evaluated using theoretical chemistry calculations. The molecular-level understanding of BrC chemistry is helpful for better understanding the evolution and behavior of light absorbing aerosols in the atmosphere.

## 1 INTRODUCTION

2 Interactions between solar radiation and atmospheric aerosols have significant yet  
3 poorly understood impact on the Earth's energy balance and climate forcing.<sup>1</sup> Understanding  
4 the chemical composition of aerosols is essential to improve the accuracy of predicting their  
5 effects in climate models.<sup>2</sup> Light-absorbing constituents of aerosols are of particular importance  
6 due to their warming effect on climate. Optical properties of the strongest light-absorbing  
7 atmospheric particles such as black carbon (BC) and mineral dust have been extensively studied  
8 in the past and have been incorporated into climate models.<sup>3, 4</sup> However, there is still  
9 substantial discrepancy between model predictions and observational data on aerosol  
10 absorption and radiative forcing.<sup>5</sup> In part, this gap may be attributed to organic aerosol  
11 components that strongly absorb solar radiation in the UV and short wavelengths of visible  
12 region.<sup>6</sup> They are collectively referred to as atmospheric "brown carbon (BrC)"<sup>6, 7</sup> because of  
13 their apparently yellow to brown color.

14 BrC is recognized as a significant contributor to light absorption and climate forcing.<sup>8</sup> In  
15 certain geographic areas or urban environments, BrC may contribute substantially or even  
16 dominate the total aerosol absorption at specific wavelengths.<sup>5, 9, 10</sup> Global models estimate  
17 that light absorption by BrC in different regions of the world may be 27%-70% of BC light  
18 absorption.<sup>11</sup> However, quantitative predictions of the BrC contribution to the overall light  
19 absorption is still a challenging task because of its compositional complexity.<sup>12, 13</sup> Numerous  
20 studies indicate that both the structure and concentration of BrC chromophores are highly  
21 variable across sources and locations.<sup>12, 13</sup> Optical properties of organic compounds strongly  
22 depend on their molecular structures. However, little is known about the fundamental  
23 relationship between the chemical composition of BrC and its light absorbing properties, which  
24 in turn results in high uncertainties in predicting and mitigating their climate effects.<sup>9, 14, 15</sup>

25 The sources of BrC are complex.<sup>12, 13</sup> BrC constituents can be present in primary aerosols  
26 emitted from combustion sources,<sup>16</sup> or they also can be formed in secondary organic aerosols  
27 (SOA) through various reaction pathways<sup>12</sup> including reactions of ammonia or amines with  
28 carbonyl compounds in SOA or cloud droplets,<sup>17, 18 19, 20</sup> dehydration of oligomers formed  
29 through reactive uptake of isoprene epoxydiols,<sup>21</sup> and photooxidation of aromatic volatile  
30 organic compounds (VOC).<sup>22-24</sup> Formation of light-absorbing nitro-aromatic compounds has  
31 been demonstrated in photooxidation of various aromatic precursors including  
32 benz[a]pyrene,<sup>25</sup> naphthalene,<sup>22</sup> catechol and guaiacol,<sup>26, 27</sup> and toluene in the presence of  
33 NO<sub>x</sub>.<sup>28, 29</sup> A theoretical study postulated that nitro- and nitrated aromatic compounds in the gas  
34 and aerosol phase may contribute significantly to light absorption within the boundary layer in  
35 the Los Angeles area.<sup>30</sup> Nitrophenols and nitrocatechols have been identified as dominant

36 light-absorbing compounds in cloud water samples and PM<sub>2.5</sub> particles impacted by biomass  
37 burning.<sup>31, 32</sup>

38 Toluene is an abundant aromatic VOC and a potential source of anthropogenic SOA  
39 formed in polluted urban air.<sup>33, 34</sup> Optical properties of SOA produced from photooxidation of  
40 toluene (Tol-SOA) in the presence of NO<sub>x</sub> have been discussed in a number of recent papers.<sup>28,</sup>  
41 <sup>29, 35-37</sup> All of these studies reported that the produced Tol-SOA exhibits substantial BrC  
42 characteristics. Light absorption by Tol-SOA in the visible range increases dramatically with  
43 increase in the initial NO<sub>x</sub> concentration in laboratory chamber experiments.<sup>28, 29</sup> Although the  
44 chemical composition of Tol-SOA has been extensively studied in the last two decades,<sup>38-41</sup> the  
45 direct correlation between light absorption and chemical composition of relevant BrC  
46 chromophores has not been established.

47 In this work, we identify and characterize chemical and light-absorbing properties of the  
48 most prominent BrC chromophores in Tol-SOA formed under high NO<sub>x</sub> conditions. We use  
49 nanospray desorption electrospray ionization (nano-DESI) to identify potential BrC  
50 chromophores. These species are subsequently analyzed using a combination of high  
51 performance liquid chromatography (HPLC) for efficient separation of Tol-SOA constituents, a  
52 UV/Vis photodiode array (PDA) detector for detection of light-absorbing molecules eluting from  
53 the HPLC column, and an electrospray ionization high-resolution mass spectrometer (ESI/HRMS)  
54 for identification of molecular formulas of individual chromophores in Tol-SOA. The LC-UV/Vis-  
55 ESI/HRMS platform allows the separation of BrC mixtures into numerous fractions with  
56 individual UV-Vis spectra (BrC chromophores) and assessment of their plausible molecular  
57 compositions. Chromophores identified in this study are representative of BrC formed in urban  
58 areas with strong anthropogenic emissions. Therefore, molecular identification of these  
59 chromophores is an important prerequisite for improved understanding of sources and aging  
60 chemistry of BrC in the atmosphere.

## 61 METHODS

62 **Generation and sampling of Toluene SOA.** Secondary organic aerosols were prepared in  
63 the PNNL 10.6 m<sup>3</sup> Teflon chamber by photooxidation of toluene in the batch mode of operation.  
64 Before each experiment, the chamber was flushed with purified air for several hours. Following  
65 cleaning, the particle concentration in the chamber was lower than 1 cm<sup>-3</sup>, and NO<sub>x</sub> was lower  
66 than 2 ppbv. Toluene was injected into the chamber by passing pure air through a gently  
67 heated glass bulb containing a measured volume of the pure compound (Sigma-Aldrich, 99.8%).  
68 Initial concentrations of toluene in the chamber were 320 ppbv. H<sub>2</sub>O<sub>2</sub> was used as OH radical  
69 precursor, and was introduced into the chamber by passing pure air over 0.5 mL H<sub>2</sub>O<sub>2</sub> (Sigma-  
70 Aldrich, 50wt% in H<sub>2</sub>O) solution. For toluene SOA samples formed under high-NO<sub>x</sub> conditions  
71 (defined here as initial NO<sub>x</sub>:toluene = 5:1), NO was injected into chamber from a gas cylinder

72 (Matheson, 500 ppm in N<sub>2</sub>). Of note, the definitions of “high NO<sub>x</sub>” and “low NO<sub>x</sub>” that we use  
 73 here are rather arbitrarily in comparison with those used in other chamber studies focused on  
 74 the estimates of SOA yields.<sup>42, 43</sup> For example, in the study of Ng et al.,<sup>43</sup> the “high NO<sub>x</sub>”  
 75 condition was reached by using NO<sub>x</sub>:toluene ≈10:1, where the peroxy radicals (RO<sub>2</sub>) reacted  
 76 only with NO. In our work here, the environmental chamber experiments were conducted to  
 77 generate two sets of the Tol-SOA samples with substantially different optical properties. Thus,  
 78 the terms of “high NO<sub>x</sub>” and “low NO<sub>x</sub>” used in this study are to distinguish these two different  
 79 samples, and emphasize effects of NO<sub>x</sub> on the formation of BrC SOA during toluene photo-  
 80 oxidation.

81 During the experiment, a suite of online instruments were used to characterize both the  
 82 gas- and particle-phase composition. The evolution of toluene concentration was tracked by an  
 83 Ionicon proton-transfer-reaction mass spectrometry (PTR-MS). For aerosols formed in the  
 84 chamber, number and volume concentrations were measured with a scanning mobility particle  
 85 spectrometer (SMPS), and mass concentration and compositions was measured by an Aerodyne  
 86 high-resolution time of flight mass spectrometry (HR-ToF-AMS). A detailed description of the  
 87 experimental and instrument operation procedures will be presented elsewhere.<sup>44</sup>

88 Tol-SOA samples were collected onto Teflon filters (Pall life sciences, 37 mm, 1 μm pore  
 89 size) for light absorption measurements. Filters were sonicated in 10 mL of high purity water  
 90 (18.2 MΩ) to extract water-soluble brown carbon. The liquid extracts were then filtered via a  
 91 25mm-diameter 0.45 μm pore syringe filter (Fisher Scientific, Fisherbrand™ Syringe Filters) to  
 92 remove insoluble components, and transferred into a Liquid Waveguide Capillary Cell  
 93 spectrophotometer to quantify the water-soluble UV-Vis light absorption spectra.<sup>45</sup> The filter  
 94 was then dried and extracted in 10 mL acetonitrile (AcN hereafter) and transferred into  
 95 spectrophotometer again to determine the light absorbance by water-insoluble components.  
 96 The solution absorption due to BrC ( $Abs(\lambda)$ , Mm<sup>-1</sup>) is determined as the sum of absorption from  
 97 both water and acetonitrile extracts, shown below,

$$98 \quad Abs_{H_2O}(\lambda) = (A_{H_2O}(\lambda) - A_{H_2O}(700)) \frac{V_l}{V_a \cdot l} \cdot \ln(10) \quad (1)$$

$$99 \quad Abs_{AcN}(\lambda) = (A_{AcN}(\lambda) - A_{AcN}(700)) \frac{V_l}{V_a \cdot l} \cdot \ln(10) \quad (2)$$

$$100 \quad Abs(\lambda) = Abs_{H_2O}(\lambda) + Abs_{AcN}(\lambda) \quad (3)$$

101 Measurements are referenced to absorption at 700nm, a region believed to be free of  
 102 absorption,<sup>16, 46</sup> to account for any signal drift.  $V_l$  is the liquid volume the filter is extracted into  
 103 (10 mL) and  $V_a$  the volume of air sampled during the filter collection period (9 L min<sup>-1</sup> for 1-3  
 104 hours).  $l$  is the waveguide optical path length (1 m in this study) and  $\ln(10)$  converts from base  
 105 10 (the form provided by the spectrophotometer) to natural logarithm. The limit of detection

106 (LOD) was  $0.066 \text{ Mm}^{-1}$ , and the uncertainty was estimated at 13%. Spectrophotometric  
107 measurements of the solution light absorption at a given wavelength ( $Abs(\lambda)$ ) were then used  
108 to determine the bulk solution mass absorption coefficient ( $MAC_{bulk}$ , in units of  $\text{m}^2 \text{g}^{-1}$ ) by,

$$109 \quad MAC_{bulk}(\lambda) = \frac{Abs(\lambda)}{M/V_a} \quad (4)$$

110 Where the aerosol loading on the filter,  $M$ , was estimated based on aerosol mass  
111 concentration measured by the AMS, the flow rate, and the sample collection time.<sup>44</sup>

112 Size-segregated Tol-SOA samples for detailed chemical analysis were collected onto a  
113 second set of Teflon substrates (Whatman, Inc.) using a ten-stage micro orifice uniform  
114 deposition impactor (MOUDI, MSP Corp., Shoreview, MN, USA) operating at a flow rate of  $30 \text{ L}$   
115  $\text{min}^{-1}$ . The Teflon filters were weighed using a microbalance before and after sampling to obtain  
116 SOA mass loadings on each filter. MOUDI was used to collect bulk aerosol samples of SOA.  
117 Samples from four stages with the highest mass loadings were used for detailed analysis.  
118 Samples of high- $\text{NO}_x$  Tol-SOA were collected on the 6<sup>th</sup> and 7<sup>th</sup> stages of MOUDI ( $0.32 \mu\text{m} < D_p <$   
119  $1.0 \mu\text{m}$ ), where  $\sim 80\%$  of the aerosol mass was deposited. In the low- $\text{NO}_x$  experiments the  
120 particle size distribution of Tol-SOA was shifted to smaller sizes, and  $\sim 80\%$  of the aerosol mass  
121 was distributed over the 7<sup>th</sup> and 8<sup>th</sup> stages ( $0.18 \mu\text{m} < D_p < 0.56 \mu\text{m}$ ) which were used for  
122 analysis, respectively. The total mass loadings collected on two stages in each of the  
123 experiments were similar between low- $\text{NO}_x$  Tol-SOA ( $230 \mu\text{g}$  on stage 7 and  $40 \mu\text{g}$  on stage 8)  
124 and high- $\text{NO}_x$  Tol-SOA ( $160 \mu\text{g}$  on stage 6 and  $110 \mu\text{g}$  on stage 7). Later, Tol-SOA materials  
125 collected on two stages were combined together and extracted for HPLC analysis. Identical  
126 solvents were used to extract Tol-SOA from filters for both the detailed chemical analysis and  
127 for the optical measurements of  $MAC_{bulk}$ .

128 **Chemical Characterization.** Tol-SOA samples were first probed directly from the  
129 substrate without any sample preparation, by using a high resolution LTQ-Orbitrap mass  
130 spectrometer (Thermo Electron, Bremen, Germany) interfaced with a custom-built nanospray  
131 desorption electrospray ionization (nano-DESI) source. Details about the experiment setup have  
132 been described in our previous studies.<sup>47, 48</sup> Briefly, the sample was positioned on a computer-  
133 controlled XYZ stage and brought in contact with the nano-DESI probe, which was assembled  
134 using two fused silica capillaries ( $50 \times 193 \mu\text{m}$ , ID  $\times$  OD, Polymicro Technologies, L.L.C., Phoenix).  
135 The solvent (50/50%, acetonitrile/water) was infused using a syringe pump at a flow rate of  $0.3-$   
136  $1 \mu\text{L}/\text{min}$  that was matched to the self-aspiration rate of the nanospray capillary.<sup>47</sup> Typical  
137 experimental conditions were: spray voltage of  $3.5 \text{ kV}$ ,  $250 \text{ }^\circ\text{C}$  temperature of the heated  
138 capillary, and the mass spectrometer was operated in the negative ion mode with a resolving  
139 power of  $\Delta m/m = 10^5$  at  $m/z$  400. The instrument was regularly calibrated using a standard  
140 calibration MSCAL 5 mixture (Sigma-Aldrich, Inc.).

141 For HPLC analysis, portions of the filter samples were extracted into 500  $\mu\text{L}$  mixtures of  
142 50/50% (v/v) acetonitrile and ultrapure water (LC-MS CHROMASOLV<sup>®</sup>, Sigma-Aldrich). Visual  
143 inspection of the filters after solvent extraction indicated that all the material was efficiently  
144 removed from the filter. The resulting solutions were first concentrated through evaporation  
145 under slow  $\text{N}_2$  flow to a volume of  $\sim 20 \mu\text{L}$ . Next,  $100 \mu\text{L}$  of ultrapure water was added to make  
146 the solvent compatible to the initial setting of solvent gradient of HPLC analysis. The mass  
147 concentration of Tol-SOA in the final solution was estimated to be approximately the same  
148  $0.56 \mu\text{g}/\mu\text{L}$  for both high and low- $\text{NO}_x$  Tol-SOA samples. The estimation was based on the  
149 measured SOA mass loading on the Teflon substrates, assuming 100% efficiency of solvent  
150 extraction.

151 Solutions containing Tol-SOA samples were subsequently analyzed using a HPLC-UV-Vis-  
152 ESI/HRMS platform for identification and characterization of the BrC chromophores. The LC/MS  
153 consists of a Surveyor Plus system (including LC pump, autosampler and PDA detector), a  
154 standard IonMAX<sup>™</sup> electrospray ionization (ESI) source, and a high resolution LTQ-Orbitrap  
155 mass spectrometer (all modules are from Thermo Electron, Inc). The separation was performed  
156 on a reverse-phase column (Luna C18,  $2 \times 150 \text{mm}$ ,  $100 \text{\AA}$  pores,  $5 \mu\text{m}$  particles, Phenomenex,  
157 Inc.). Gradient elution was performed by  $\text{H}_2\text{O}/\text{AcN}$  at a flow rate of  $200 \mu\text{L min}^{-1}$ : 0-3 min hold  
158 at 10% of AcN, 3-43 min linear gradient to 90% AcN, 43-50 min hold this level, 50-51 min back  
159 to 10% AcN, and hold until 70 min to recondition the column and make it ready for injection of  
160 the next sample. UV/vis absorption was measured using PDA over the wavelength range of 200  
161 to 700 nm. The ESI setting were:  $-3.5 \text{kV}$  spray potential, 35 units of sheath gas flow, 10 units of  
162 auxiliary gas flow, and 8 units of sweep gas flow.

163 Xcalibur (Thermo Scientific) was used to acquire raw data. Mass spectral features with a  
164 minimum signal-to-noise ratio of 10 were extracted by using Decon2LS software<sup>49</sup> developed at  
165 Pacific Northwest National Laboratory (PNNL) (<http://ncrr.pnl.gov/software/>). Data processing  
166 was performed using a suite of Microsoft Excel macros developed in our group, including  
167 background subtraction, first and second-order Kendrick mass defect analysis. Details about  
168 these procedures have been described in our previous studies.<sup>50, 51</sup> Elemental formulas were  
169 assigned to one peak in each group using MIDAS molecular formula calculator  
170 (<http://magnet.fsu.edu/~midas/>). Formula assignments were performed using the following  
171 constraints:  $\text{C} \leq 50$ ,  $\text{H} \leq 100$ ,  $\text{N} \leq 5$ , and  $\text{O} \leq 50$ . Neutral formulas were obtained by adding a  
172 proton to the formulas of  $[\text{M}-\text{H}]^+$  ions. The double-bond equivalent (DBE) of the neutral  
173 formulas was calculated using the equation:  $\text{DBE} = c - h/2 + n/2 + 1$ . Where  $c$ ,  $h$ , and  $n$   
174 correspond to the number of carbon, hydrogen and nitrogen atoms in the neutral formula,  
175 respectively.

176 **Chemical Structure and UV/vis Calculations.** The quantum chemical calculations of the  
177 optimized structures and UV/vis absorption spectra were performed using the Gaussian  
178 software package.<sup>52</sup> As a balance between accuracy and computational efficiency, the B3LYP/6-  
179 311++G\*\* level of theory and basis sets were employed for both geometry optimizations and  
180 the TD-DFT UV/vis calculations of the first 20 excited singlet electronic states.<sup>53</sup> Solvent effects  
181 were not included since we were looking for general trends in the behavior of the UV/vis  
182 spectra on the location of the specific functional groups around the aromatic rings of the  
183 spectral candidates relevant to BrC. The suitability of the selected quantum chemistry method  
184 was tested by performing a series of calculations for selected aromatic compounds of  
185 increasing complexity to ensure the calculated UV/vis trends were correct. The series included  
186 naphthalene, anthracene, and tetracene. The computed trends of maximum absorption ( $\lambda_{\max}$ )  
187 between these compounds matched well their corresponding literature values.<sup>54</sup> Specifically,  
188 the calculated (literature) values were: naphthalene = 285nm (301nm), anthracene = 383nm  
189 (376nm), and tetracene = 500nm (474nm). Thus, the level of theory and the basis sets selected  
190 for our study were sufficient to reproduce trends quite well.

191

## 192 RESULTS AND DISCUSSIONS

193 Samples of Tol-SOA produced under high and low  $\text{NO}_x$  conditions have substantially  
194 different light absorbing properties as inferred from both visual observations and  $\text{MAC}_{\text{bulk}}$   
195 measurements. Figure 1 shows photographs of the high- and low- $\text{NO}_x$  Tol-SOA samples along  
196 with a plot indicating differences in their  $\text{MAC}_{\text{bulk}}$  values. It is observed that the sample of high-  
197  $\text{NO}_x$  Tol-SOA appears yellow in color and exhibits significant light absorption at near UV and  
198 short visible wavelength with  $\text{MAC}_{\text{bulk}@365\text{nm}} = 0.78 \text{ m}^2 \text{ g}^{-1}$ . In contrast, Tol-SOA produced  
199 under low- $\text{NO}_x$  conditions is colorless, and its  $\text{MAC}_{\text{bulk}@365\text{nm}}$  value of  $0.01 \text{ m}^2 \text{ g}^{-1}$  is almost  
200 two orders of magnitudes lower than that of the high- $\text{NO}_x$  Tol-SOA. These two samples were  
201 further analyzed to obtain detailed information on the chemical composition and the light  
202 absorption properties of the individual molecular components.

203 **Compositional differences between Tol-SOA generated under high- and low- $\text{NO}_x$**   
204 **conditions.** The Tol-SOA samples were first analyzed by nano-DESI/HRMS to obtain an overview  
205 of their molecular composition. Figure 2 shows mass spectra of Tol-SOA generated at high- $\text{NO}_x$   
206 and low- $\text{NO}_x$  conditions. The chemical composition of Tol-SOA generated under high- $\text{NO}_x$   
207 conditions is remarkably different from that formed under low- $\text{NO}_x$  conditions. A large number  
208 of nitrogen containing compounds (CHON) were produced under high- $\text{NO}_x$  conditions, and  
209 accounted for ~68% of the assigned elemental formulas. A majority of the CHON molecules  
210 (~90%) have O/N ratios higher than 2, consistent with the assumption that those products  
211 contain at least one nitro group ( $-\text{NO}_2$ ). The candidates for these CHON compounds include

212 nitro-phenol analogues, organic nitrates, acylperoxyl nitrates, and unsaturated hydroxyl nitro  
213 acids, which can overall account for > 60% of aerosol mass in tol-SOA, as predicted by the  
214 kinetic mechanism of photochemical oxidation of toluene.<sup>55</sup> In contrast, photooxidation  
215 products observed in Tol-SOA produced under low-NO<sub>x</sub> conditions are dominated by  
216 compounds composed of carbon, hydrogen and oxygen atoms (CHO). Although some of the  
217 CHON compounds were also detected in low-NO<sub>x</sub> Tol-SOA, they were only observed as ions  
218 with very low intensities (signal/noise ratio < 80). Those compounds are likely products of SOA  
219 carbonyl compounds reacting with NH<sub>3</sub> during exposure of samples to an ambient air at the  
220 time of sample handling and data acquisition.<sup>17,47</sup>

221 The compositional diversity of Tol-SOA components and their dependence on the initial  
222 concentration of NO<sub>x</sub> reflects differences in mechanisms of toluene oxidation by mixed OH/NO<sub>x</sub>  
223 oxidants. Oxidation of toluene initiated by reactions with OH radical has been studied by  
224 several groups.<sup>38-41, 55-57</sup> For instance, Forstner et al.<sup>38</sup> reported that about 90% of products  
225 were formed through OH radical addition resulting in formation of methyl hydroxyl  
226 cyclohexadieny radicals, which may further react with O<sub>2</sub> ( $k \approx 5 \times 10^{-16} \text{ cm}^3 \text{ molecule}^{-1} \text{ s}^{-1}$ ) or NO<sub>2</sub>  
227 ( $k \approx 3 \times 10^{-11} \text{ cm}^3 \text{ molecule}^{-1} \text{ s}^{-1}$ ).<sup>57, 58</sup> It is reported that the reaction with O<sub>2</sub> leads to a series of  
228 fragmentation, rearrangement, and radical propagation products with CHO composition such as  
229 reactive aldehydes, carboxylic acids, quinoid and furanoid compounds.<sup>39, 56</sup> Under common  
230 tropospheric conditions, the O<sub>2</sub> pathway typically dominates.<sup>57</sup> However, when NO<sub>x</sub>  
231 concentrations are high, a fraction of the cyclohexadienyl radicals noted above react by  
232 addition of NO<sub>2</sub><sup>41</sup> to the aromatic ring leading to formation of nitro aromatic compounds.<sup>39</sup>  
233 Though this pathway likely represents a small subset of all reactions, it does not lead to  
234 fragmentation and therefore may contribute substantially to SOA mass.

235 Additionally, about 10% of toluene oxidation products are formed through H-atom  
236 abstraction of the methyl group and results in formation of benzaldehydes, which can further  
237 oxidize to lower volatility benzoic acid<sup>38</sup> that partitions into particle phase. In the condensed  
238 phase, benzoic acids and benzaldehydes may participate in oligomerization reactions yielding  
239 higher molecular weight (high-MW) products.<sup>59</sup> In contrast, at high-NO<sub>x</sub> conditions, reaction  
240 products are shifted towards formation of nitrophenols<sup>39</sup> that have lower tendency for  
241 fragmentation and oligomerization.

242 A variety of organic radicals are produced through radical propagation reactions during  
243 toluene oxidation. These organic radicals may also react with NO<sub>2</sub> and lead to nitrogen  
244 containing products. For instance, it was estimated that the effective yield of the reaction  
245 between methyl phenoxy radicals and NO<sub>2</sub> increased from 0.34 to 0.69 as the effective NO<sub>2</sub>  
246 concentration increased from 13 to 97 ppbv,<sup>28</sup> demonstrating the overwhelming reaction with

247 NO<sub>2</sub> rather than with other oxidants. The reactions of organic radicals with NO<sub>x</sub> regulate the  
248 amount of nitrogen containing compounds formed in Tol-SOA as illustrated by Figure 2.

249 Figure 2 indicates that Tol-SOA produced under low-NO<sub>x</sub> conditions contain a larger  
250 fraction of high-MW products in comparison with Tol-SOA formed under high-NO<sub>x</sub>. These high-  
251 MW species are mainly CHO compounds. As we mentioned before, the O<sub>2</sub> pathway leads to a  
252 series of radical propagation reactions and results in a variety of aldehydes and organic peroxy  
253 radicals (RO<sub>2</sub>). High-MW compounds are formed from these reactive aldehydes through  
254 hemiacetal/acetal oligomerization and/or aldol condensation.<sup>59, 60</sup> Under high-NO<sub>x</sub> conditions,  
255 the addition of NO<sub>2</sub> to organic radicals terminate radical propagation, which result in more ring-  
256 retaining products and less aldehydes that may not favor oligomerization. Under low NO<sub>x</sub>  
257 conditions, RO<sub>2</sub> radicals react with hydroperoxyl radical (HO<sub>2</sub>), forming organic hydroperoxides  
258 (ROOH) that may further react with aldehyde species to produce low volatile peroxy  
259 hemiacetals, which play an important role in SOA formation.<sup>61</sup> In contrast, under high NO<sub>x</sub>  
260 conditions, RO<sub>2</sub> radicals react with NO<sub>x</sub> to produce species which are less likely to undergo  
261 particle-phase oligomerization reactions that contribute to the formation of high-MW products.  
262 In summary, comparison of nano-DESI spectra of Tol-SOA produced under low-NO<sub>x</sub> and high-  
263 NO<sub>x</sub> conditions suggests that nitrogen-containing species abundant in the high-NO<sub>x</sub> Tol-SOA  
264 may contribute to the observed light absorption while oligomeric products abundant in the  
265 low-NO<sub>x</sub> Tol-SOA do not absorb visible light to a significant extent.

266 UV/Vis absorption spectra of organic molecules vary dramatically with their structural  
267 features. The extent of the double bond conjugation that can be indirectly inferred from a  
268 number of double bonds and rings in the molecule expressed as DBE is an important parameter  
269 that determines molecular optical properties.<sup>62</sup> Figure 3 shows the DBE values for compounds  
270 observed in the high-NO<sub>x</sub> and low-NO<sub>x</sub> Tol-SOA plotted as a function of a number of carbon  
271 atoms. The upper compositional boundary for naturally occurring hydrocarbons in fossil resources<sup>63</sup> is  
272 shown by the blue line. The extent of unsaturation and conjugation in each identified product  
273 can be inferred from this plot. Specifically, oxidation products observed in Tol-SOA generated  
274 under high- NO<sub>x</sub> conditions have higher extent of unsaturation in comparison to compounds  
275 observed in Tol-SOA generated under low-NO<sub>x</sub> conditions. This is consistent with previous work  
276 by Birdsall et al<sup>64</sup> showing that a larger fraction of aromatic products are present in high-NO<sub>x</sub>  
277 Tol-SOA, while under low-NO<sub>x</sub> conditions, the addition of O<sub>2</sub> initiates a series of radical  
278 propagation reactions leading to a variety of ring cleavage products. Higher degree of  
279 conjugation tends to reduce the energy gap for  $\pi \rightarrow \pi^*$  transitions, leading to light absorption at  
280 longer wavelengths. In addition, light absorption by organic molecules is also affected by  
281 functional groups. For example, it is well-established that absorption of visible light is often  
282 enhanced in the presence of nitro/nitrate groups in the molecule.<sup>65</sup> As discussed earlier,  
283 nitroaromatic compounds have been identified as the dominant light-absorbing species in field-

284 collected aerosol samples.<sup>31, 32</sup> However, detailed speciation of the light-absorbing molecules in  
285 Tol-SOA has not been previously reported. In the following section we describe chemical  
286 characterization of the individual BrC chromophores in Tol-SOA using HPLC-UV/Vis-ESI/HRMS.

287 **Identification of BrC chromophores.** Figure 4 shows UV/Vis chromatograms integrated  
288 over the 300-500nm region and MS total ion count (TIC) chromatograms obtained by HPLC  
289 analysis of both high-NO<sub>x</sub> and low-NO<sub>x</sub> Tol-SOA samples. The results demonstrate that the high-  
290 NO<sub>x</sub> Tol-SOA sample contains a number of well-separated molecular fractions that efficiently  
291 absorb light in the 300-500nm region. In contrast, a very different UV/Vis chromatogram was  
292 obtained for the low-NO<sub>x</sub> Tol-SOA sample with only several small features observed above the  
293 background. Similarly, the TIC chromatogram obtained for the high-NO<sub>x</sub> sample exhibits distinct  
294 features in comparison to that of the low-NO<sub>x</sub> sample (Figure 4). After correcting for the shift in  
295 retention times (RT) between the signals recorded by MS and UV/Vis detectors, the major  
296 absorption peaks in the UV/Vis chromatogram were found to correlate well with the major  
297 peaks observed in the TIC chromatogram, suggesting that ions contributing to the MS signal are  
298 also responsible for signals detected by the PDA detector.

299 The mass spectrum of each chromatographic peak usually contains a number of ions  
300 corresponding to the analyte of interest as well as to the solvent background and species that  
301 were not separated by HPLC. We used comparative analysis of MS spectra recorded at the  
302 beginning, maximum, and end of the chromatographic feature to identify ion signals strongly  
303 correlated with the UV/Vis chromatographic peaks. Details of the data analysis methodology  
304 are elaborated in the SI file (see Figure S1 and the associated text).

305 Figure 5 shows extracted ion chromatograms (EIC) of selected abundant ions that  
306 correlate with the features in the UV/Vis chromatogram of the high-NO<sub>x</sub> Tol-SOA sample. A  
307 majority of these compounds contain 6-7 carbon atoms with DBE values ranging from 5 to 7,  
308 indicative of the preserved aromatic ring. In addition, there are also 1-3 nitrogen atoms and 3-7  
309 oxygen atoms in each molecule, making O/N ratio greater than 2 in all of the identified species.  
310 These observations suggest that these compounds most likely contain nitro group, an  
311 assumption that explains DBE values in excess of 4 (characteristic for a single aromatic ring).

312 A summary of the most prominent BrC chromophores, their UV/Vis spectra and  
313 corresponding retention times (RT) is listed in Table 1. Overall, 15 major BrC features along with  
314 their elemental composition were identified and their plausible molecular structures were  
315 suggested. Several commercially available compounds such as picnic acid and 3,5-  
316 dinitrosalicylic acid were analyzed using the same experimental conditions. This allowed a  
317 direct comparison of their UV/Vis spectra and retention times with the features observed in the  
318 high-NO<sub>x</sub> Tol-SOA sample. In addition, we were able to identify several compounds by  
319 comparing their elemental composition with the composition of toluene photooxidation

320 products identified in previous studies and their UV/Vis spectra with UV/Vis spectra of  
321 individual compounds reported in literature. For example, the UV/Vis spectrum of the peak that  
322 eluted at 16.5min is characterized by maximum absorption ( $\lambda_{\max}$ ) at 347nm and a shoulder  
323 around 310nm. Based on the HRMS data, the compound eluted at this time was assigned with  
324 neutral elemental formula  $C_6H_5NO_4$ , which is most likely nitrocatechol. The UV/Vis spectrum of  
325 4-nitrocatechol was reported with  $\lambda_{\max}$  at 345nm and a shoulder at 309nm.<sup>66</sup> In contrast,  
326 another isomer, 3-nitrocatechol was reported with  $\lambda_{\max}$  at 296nm.<sup>67</sup> Based on this comparison  
327 we identified the chromophore eluting at 16.5 min as 4-nitrocatechol.

328 We note that in some cases, the observed UV-Vis spectrum may be a combination of the  
329 UV/vis spectra of several compounds. For example, absorbance at RT = 24.3 min correlates well  
330 with the elution time of two molecules with elemental formula of  $C_7H_7NO_3$  and  $C_6H_4N_2O_5$ ,  
331 respectively. Nitrocresols ( $C_7H_7NO_3$ ) have been identified in Tol-SOA produced in the presence  
332 of  $NO_x$ .<sup>39</sup> One of its isomers, 4-nitro-o-cresol, has peak absorption wavelength ( $\lambda_p$ ) at 319nm,<sup>30</sup>  
333 which is close to  $\lambda_p$  (325nm) of the spectrum observed at RT = 24.3min (Table 1). The minor red-  
334 shift of the observed absorption may be caused by co-eluted  $C_6H_4N_2O_5$ , probably dinitrophenol.  
335 Some of its isomers, e.g., 2,6-dinitrophenol and 2,3-dinitrophenol, absorb light at longer  
336 wavelengths of 350 and 329 nm, respectively<sup>30</sup> and could contribute to the observed  
337 absorption.

338 There are two elemental formulas corresponding to the compounds eluted at RT =  
339 21.7min:  $C_7H_7NO_4$  and  $C_6H_4N_2O_6$ , which are likely methyl-nitrocatechol<sup>40</sup> and dinitrocatechol,<sup>68</sup>  
340 respectively. The PDA spectrum at this RT appeared to be similar to that eluted at 16.5min,  
341 which was mainly contributed by nitrocatechol. Moreover, for each identified formula, multiple  
342 structural isomers are possible. In order to assess the effect of methyl-substitution and  
343 functional groups' positions on the UV/Vis spectra of aromatic compounds, the spectroscopic  
344 properties of several model compounds were evaluated by quantum chemistry calculations of  
345 their electronic structures.<sup>53</sup> Figure S2 shows the chemical structures of the 14 model  
346 compounds and their absorption spectra obtained from quantum calculations. Table 1 includes  
347 several conclusions that were drawn from these results. First, the substitution of methyl group  
348 and its position on the aromatic ring doesn't change substantially the UV/Vis spectra of  
349 aromatic compounds, as demonstrated by comparing the structures 1 – 3 of Figure S2. Second,  
350 the UV/Vis spectra of structures 4-7 suggest that the relative positions of  $-OH$  and  $-NO_2$  groups  
351 on the aromatic ring significantly affect the absorbance of nitrocatechol. Similar effects were  
352 also found for the isomers of dinitrocatechol (structures 8-14). The calculated results indicate  
353 that molecular structures with  $-NO_2$  groups in *para* positions have the longest wavelength of  
354 light absorbance, followed by *ortho* and *meta* isomers. The position of  $-OH$  groups have  
355 additional but less pronounced influence. In the end, we should point out that all the  
356 theoretical calculations used here are applied for single molecule only, without taking into

357 account the solute-solvent interactions, which were suggested to have a direct and significant  
358 influence on the UV/Vis spectra.<sup>66</sup> This makes it difficult to directly compare the spectra  
359 measured by PDA with those calculated by quantum methods. However, the quantum chemical  
360 calculations do provide important trends as to the effect of different locations of the functional  
361 groups around the aromatic rings on the UV/vis spectra. The key result of these calculations  
362 indicate that when the nitro groups are farthest apart, i.e., on opposite sides of the aromatic  
363 ring, the HOMO-LUMO gap is reduced yielding absorption wavelengths that are red-shifted  
364 with respect to compounds with adjacent nitro groups. This can be easily understood via the  
365 well-known quantum particle in a box – larger boxes allow for absorption at longer wavelengths.

366 Figure 6 illustrates analysis results in two cases where identification of BrC features was  
367 assisted by comparison with commercially available standards. Specifically, the compound with  
368 assigned elemental formula  $C_6H_3N_3O_7$  was identified as the most abundant ion eluted at RT =  
369 39.1 min, while the signals of other ions with the same chromatographic record were  
370 substantially lower. The EIC of these ions correlate well with the UV/Vis signal (Figure 6a). In  
371 ESI-MS, the intensity of ion signal is determined by both concentration and ionization efficiency  
372 of the analyte molecule. Therefore, it is hard to unambiguously conclude whether the signal  
373 intensities of these compounds, as shown in Figure 6a, represent their relative concentrations  
374 in the mixture and relative contribution to UV/Vis absorbance. However, in this case it was  
375 possible to compare the UV/Vis spectrum of this BrC feature with a commercially available  
376 standard of picric acid ( $C_6H_3N_3O_7$ ). As shown in Figure 6c, the corresponding two spectra match  
377 very well with each other. The result implies that picric acid is most likely the dominant BrC  
378 chromophore responsible for light absorption at RT = 39.1 min.

379 Figure 6b shows another example of BrC chromophore eluting at RT = 36.9min, where  
380 two major ions (with neutral formulas  $C_7H_4N_2O_7$  and  $C_6H_4N_2O_5$ ) along with several low-  
381 abundance species were detected. The UV/Vis spectrum of this BrC feature was found to  
382 match well with the spectrum of 3, 5-dinitrosalicylic acid ( $C_7H_4N_2O_7$ ) (Figure 6d). The latter was  
383 also analyzed with LC-MS using the same experimental conditions and was found to elute at  
384 similar retention time. The mass spectrum of 3, 5-dinitrosalicylic acid also contained both  
385  $C_7H_4N_2O_7$  and  $C_6H_4N_2O_5$  suggesting that  $C_6H_4N_2O_5$  is a fragment of  $C_7H_4N_2O_7$  formed in the ESI  
386 process or through in-source fragmentation. It follows that 3, 5-dinitrosalicylic acid is the  
387 characteristic BrC chromophore responsible for light absorption at RT = 36.9 min.

388 The results shown in Figures 5 and 6 indicate that the most abundant ions observed in  
389 MS determined the light absorption observed by UV/Vis. The absorption spectra of 15  
390 identified peaks from Table 1 were summed together to evaluate their contributions to the  
391 total absorption measured by PDA detector as shown in Figure 7. The total absorbance of these  
392 15 peaks accounts for 60% and 41% of the overall absorbance in the wavelength ranges of 300-

393 400nm and 400-500nm, respectively. The rest of the absorption is mainly due to the rising  
394 baseline or a broad “hump” observed in the UV/vis chromatogram at 15-30min (Figure 4, blue  
395 line). This chromatographic feature is similar to those frequently observed in gas  
396 chromatography (GC) data of atmospheric aerosols<sup>69, 70</sup> or other complex organic mixtures,  
397 where a term unresolved complex mixtures (UCM) was introduced.<sup>71</sup> The mass spectra of LC  
398 fractions eluted within this period were averaged and processed following the same  
399 methodology described in Figure S1 of the SI file. The resulting mass spectrum consisted of over  
400 100 ions, including 11 of the identified chromophores from Table 1 as the most abundant ions  
401 (see Figure S2 of the SI file). The intensities of other ions were substantially smaller than the  
402 intensities of the identified ions, indicating either their low individual concentrations or poor  
403 ionization efficiency. It is also possible that some chromophores detected by PDA are not  
404 ionized by ESI. Further identification of chromophores in the UCM fraction is still challenging  
405 and may require two-dimensional chromatographic technology,<sup>72</sup> which is beyond our current  
406 instrumental capability.

407 Figure 7 also illustrates that among 15 identified chromophores, light absorption above  
408 350 nm is dominated by 10 peaks eluting between 14-40 min. As shown in Table 1,  
409 chromophores eluting during this period are mainly nitro-phenolic compounds. It is interesting  
410 to note that the UCM fraction also elutes at the same time (i.e., 15-30min). This observation  
411 suggests that compounds in the UCM fraction have similar physiochemical properties as the  
412 abundant chromophores identified in this study, which may explain the substantial light  
413 absorption by UCM. We assigned molecular formulas to the observed ions in the UCM fraction  
414 as described in the experimental section. Overall, 98 ions were successfully assigned with  
415 reasonable formulas within the constraints used in this study ( $C \leq 50$ ,  $H \leq 100$ ,  $N \leq 5$ , and  $O \leq$   
416  $50$ ). Unambiguous formula assignment of other peaks was not possible either due to the  
417 reduced mass accuracy for low-intensity peaks or because of the presence of other elements  
418 not considered in our assignment. 78 of the 98 identified formulas are CHON compounds with  
419 O/N ratio greater than 2, and 92 compounds contain at least six carbon atoms and have DBE/C >  
420 0.5, suggesting the presence of nitro/nitrate groups and aromatic structures. It follows that  
421 chromophores in the UCM fraction are also predominately nitro-aromatic and/or organonitrate  
422 compounds.

423 **Atmospheric implications.** The combination of HPLC with UV/Vis spectroscopy and  
424 ESI/HRMS is shown to be an effective analytical platform for the identification of BrC  
425 chromophores and characterization of their light-absorption properties. Tol-SOA, selected as  
426 one of the best characterized secondary BrC aerosols, were examined in this study. The results  
427 provide direct evidence that nitro-phenols are significant BrC chromophores responsible for the  
428 enhanced BrC characteristics of Tol-SOA generated under high-NO<sub>x</sub> conditions. Considering that  
429 both aromatic hydrocarbons and NO<sub>x</sub> are substantial anthropogenic air pollutants in urban

430 regions,<sup>73</sup> nitro-phenolic compounds produced from the photo-oxidation of aromatic  
431 hydrocarbons could be an important source of BrC in urban atmosphere.

432 In this study, BrC SOA was produced in a smog chamber simulating the daytime  
433 troposphere photochemistry, and nitro-phenols were identified as significant BrC  
434 chromophores. It should be pointed out that, besides daytime gas-phase chemistry, there are  
435 also other atmospheric processes or emission sources that can produce nitro-phenols. Such  
436 processes/sources include nighttime <sup>•</sup>NO<sub>3</sub>-mediated nitration of phenols in the gas phase,<sup>74</sup>  
437 hydroxylation and nitration of aqueous benzene in the presence of nitrite under UV-  
438 irradiation,<sup>75</sup> combustion processes of motor vehicles,<sup>76</sup> and biomass burning.<sup>31, 32, 77</sup> A recent  
439 study of Liu et al. reported that the imaginary part (*k*) of refractive indices ( $m = n - ik$ ) of the  
440 aromatic SOA produced from photooxidation of toluene and m-xylene in the presence of NO<sub>x</sub> is  
441 similar to those reported for BrC in urban and biomass burning plumes.<sup>29</sup> The conclusions of  
442 these studies expand the significance of nitro-phenolic compounds as BrC chromophores in the  
443 atmosphere.

444 It is important to point out that most of these nitro-phenolic compounds are acidic in  
445 nature and deprotonation of the neutral BrC chromophores may have significant effect on their  
446 absorption spectra.<sup>78</sup> Table 2 lists several nitro-phenolic compounds with known acid  
447 dissociation constants (pKa) and their longest peak UV/Vis absorption wavelength ( $\lambda_p$ ). It is  
448 shown that the deprotonated forms of these compounds usually absorb at considerably longer  
449 wavelength than their neutral counterparts. Molar (or mass) absorption coefficients also vary  
450 greatly for deprotonated and protonated forms of molecules. Deprotonation of an acidic  
451 compound depends on its pKa and the pH of the solution.<sup>79</sup> The pH of cloud and fog droplets  
452 was measured in a wide range of 2.3-7.6.<sup>80, 81</sup> Aerosol in-situ pH cannot be directly measured  
453 due to its low liquid water content (LWC), but can be estimated by thermodynamic models.<sup>82, 83</sup>  
454 In urban area, the in-situ pH of ambient aerosols is generally acidic (pH < 4.0),<sup>84, 85</sup> regulated by  
455 the molar ratio of major inorganic components and LWC.<sup>86</sup> Since the pKa values of nitro-  
456 phenolic compounds are close to or within the range of atmospheric pH, their light absorption  
457 spectra may be significantly affected by changes in the acidity of aerosol population.

458 Despite the acidic nature of SOA produced from gas- and aqueous-phase oxidation  
459 processes in urban atmosphere, another class of light absorbing aerosol, mineral dust, is mainly  
460 composed of alkaline components. Mineral dust aerosols can transport over thousands  
461 kilometers from their source regions and account for a larger fraction of aerosol flux on global  
462 scale. The alkaline components of mineral dust have shown great capacity to buffer the acidity  
463 of rain water.<sup>87, 88</sup> The acidity of SOA may be neutralized in the same way when they mixed with  
464 mineral dust or marine aerosols.<sup>89-91</sup> As a result, the light absorption properties of BrC SOA may  
465 also be modified. In the case of tol-SOA, its BrC characteristics are enhanced during this process.

466 We propose that the pH dependence of light absorption characteristics may be an important  
467 property of BrC aerosols that need to be systematically investigated in future studies.

468 **ACKNOWLEDGEMENT**

469 Authors acknowledge support by the Laboratory Directed Research and Development  
470 funds of Pacific Northwest National Laboratory (PNNL). We thank Dr. Marat Valiev for fruitful  
471 discussions of the calculated results. The HPLC-UV/Vis-ESI/HRMS experiments were performed  
472 at the William R. Wiley Environmental Molecular Sciences Laboratory, a national scientific user  
473 facility sponsored by the DOE's Office of Biological and Environmental Research and located at  
474 PNNL. PNNL is operated for the U.S. Department of Energy by Battelle Memorial Institute under  
475 Contract No. DE-AC06-76RLO 1830.

476

477

## 478 References:

- 479 1. IPCC, *Fourth Assessment Record: Climate Change 2007*, Cambridge University Press, New York,  
480 2007.
- 481 2. J. H. Seinfeld and S. N. Pandis, *Atmospheric Chemistry and Physics: From Air Pollution to Climate*  
482 *Change*, Wiley-Interscience; 2 edition, 2006.
- 483 3. T. C. Bond, C. Zarzycki, M. G. Flanner and D. M. Koch, *Atmos Chem Phys*, 2011, **11**, 1505-1525.
- 484 4. X. Ma, F. Yu and G. Luo, *Atmos Chem Phys*, 2012, **12**, 5563-5581.
- 485 5. C. E. Chung, V. Ramanathan and D. Decremmer, *P Natl Acad Sci USA*, 2012, **109**, 11624-11629.
- 486 6. M. O. Andreae and A. Gelencser, *Atmos Chem Phys*, 2006, **6**, 3131-3148.
- 487 7. P. Formenti, W. Elbert, W. Maenhaut, J. Haywood, S. Osborne and M. O. Andreae, *J Geophys*  
488 *Res-Atmos*, 2003, **108**, 8488.
- 489 8. Y. Feng, V. Ramanathan and V. R. Kotamarthi, *Atmos Chem Phys*, 2013, **13**, 8607-8621.
- 490 9. R. Bahadur, P. S. Praveen, Y. Y. Xu and V. Ramanathan, *P Natl Acad Sci USA*, 2012, **109**, 17366-  
491 17371.
- 492 10. V. Ramanathan, F. Li, M. V. Ramana, P. S. Praveen, D. Kim, C. E. Corrigan, H. Nguyen, E. A. Stone,  
493 J. J. Schauer, G. R. Carmichael, B. Adhikary and S. C. Yoon, *J Geophys Res-Atmos*, 2007, **112**,  
494 D22S21.
- 495 11. G. X. Lin, J. E. Penner, M. G. Flanner, S. Sillman, L. Xu and C. Zhou, *J Geophys Res-Atmos*, 2014,  
496 **119**, 7453-7476.
- 497 12. T. Moise, J. Michel Flores and Y. Rudich, *chemical reviews*, 2015, **115**, 4400-4439.
- 498 13. A. Laskin, J. Laskin and S. A. Nizkorodov, *Chemical Reviews*, 2015, **115**, 4335-4382.
- 499 14. D. T. L. Alexander, P. A. Crozier and J. R. Anderson, *Science*, 2008, **321**, 833-836.
- 500 15. T. C. Bond and R. W. Bergstrom, *Aerosol Sci Tech*, 2006, **40**, 27-67.
- 501 16. Y. Chen and T. C. Bond, *Atmos Chem Phys*, 2010, **10**, 1773-1787.
- 502 17. J. Laskin, A. Laskin, P. J. Roach, G. W. Slysz, G. A. Anderson, S. A. Nizkorodov, D. L. Bones and L. Q.  
503 Nguyen, *Anal Chem*, 2010, **82**, 2048-2058.
- 504 18. K. M. Updyke, T. B. Nguyen and S. A. Nizkorodov, *Atmos Environ*, 2012, **63**, 22-31.
- 505 19. A. K. Y. Lee, R. Zhao, R. Li, J. Liggio, S. M. Li and J. P. D. Abbatt, *Environ Sci Technol*, 2013, **47**,  
506 12819-12826.
- 507 20. M. H. Powelson, B. M. Espelien, L. N. Hawkins, M. M. Galloway and D. O. De Haan, *Environ Sci*  
508 *Technol*, 2014, **48**, 985-993.
- 509 21. Y. H. Lin, H. Budisulistiorini, K. Chu, R. A. Siejack, H. F. Zhang, M. Riva, Z. F. Zhang, A. Gold, K. E.  
510 Kautzman and J. D. Surratt, *Environ Sci Technol*, 2014, **48**, 12012-12021.
- 511 22. A. T. Lambe, C. D. Cappa, P. Massoli, T. B. Onasch, S. D. Forestieri, A. T. Martin, M. J. Cummings,  
512 D. R. Croasdale, W. H. Brune, D. R. Worsnop and P. Davidovits, *Environ Sci Technol*, 2013, **47**,  
513 6349-6357.
- 514 23. H. J. Lee, P. K. Aiona, A. Laskin, J. Laskin and S. A. Nizkorodov, *Environ Sci Technol*, 2014, **48**,  
515 10217-10226.
- 516 24. S. Liu, J. E. Shilling, C. Song, N. Hiranuma, R. A. Zaveri and L. M. Russell, *Aerosol Sci Tech*, 2012,  
517 **46**, 1359-1369.
- 518 25. J. W. Lu, J. M. Flores, A. Lavi, A. Abo-Riziq and Y. Rudich, *Phys Chem Chem Phys*, 2011, **13**, 6484-  
519 6492.
- 520 26. Z. Kitanovski, A. Cusak, I. Grgic and M. Claeys, *Atmos Meas Tech*, 2014, **7**, 2457-2470.
- 521 27. J. Ofner, H. U. Kruger, H. Grothe, P. Schmitt-Kopplin, K. Whitmore and C. Zetzsch, *Atmos Chem*  
522 *Phys*, 2011, **11**, 1-15.
- 523 28. T. Nakayama, K. Sato, Y. Matsumi, T. Imamura, A. Yamazaki and A. Uchiyama, *Atmos Chem Phys*,  
524 2013, **13**, 531-545.

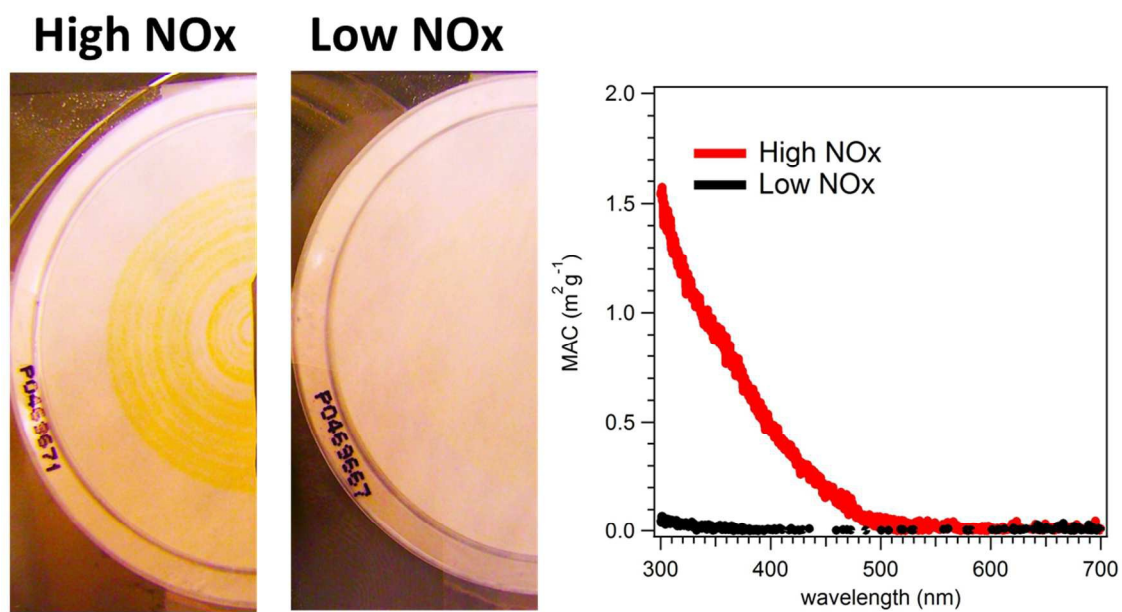
- 525 29. P. F. Liu, N. Abdelmalki, H.-M. Hung, Y. Wang, W. H. Brune and A. T. Martin, *Atmos. Chem. Phys.*,  
526 2015, **15**, 1435-1436.
- 527 30. M. Z. Jacobson, *J Geophys Res-Atmos*, 1999, **104**, 3527-3542.
- 528 31. M. Claeys, R. Vermeylen, F. Yasmeen, Y. Gomez-Gonzalez, X. G. Chi, W. Maenhaut, T. Meszaros  
529 and I. Salma, *Environ Chem*, 2012, **9**, 273-284.
- 530 32. Y. Desyaterik, Y. Sun, X. H. Shen, T. Y. Lee, X. F. Wang, T. Wang and J. L. Collett, *J Geophys Res-*  
531 *Atmos*, 2013, **118**, 7389-7399.
- 532 33. S. D. Piccot, J. J. Watson and J. W. Jones, *J Geophys Res-Atmos*, 1992, **97**, 9897-9912.
- 533 34. Jack G. Calvert, Roger Atkinson, Karl H. Becker, Richard M. Kamens, John H. Seinfeld, Timonthy H.  
534 Wallington and G. Yarwood, *The Mechanisms of Atmospheric Oxidation of the Aromatic*  
535 *Hydrocarbons*, Oxford University Press, New York, 2002.
- 536 35. H. Kim and S. E. Paulson, *Atmos Chem Phys*, 2013, **13**, 7711-7723.
- 537 36. K. Li, W. Wang, M. Ge, J. Li and D. Wang, *Sci. Rep.*, 2014, **4**, 4922.
- 538 37. M. Zhong and M. Jang, *Atmos Environ*, 2011, **45**, 4263-4271.
- 539 38. H. J. L. Forstner, R. C. Flagan and J. H. Seinfeld, *Environ Sci Technol*, 1997, **31**, 1345-1358.
- 540 39. M. S. Jang and R. M. Kamens, *Environ Sci Technol*, 2001, **35**, 3626-3639.
- 541 40. J. L. Kelly, D. V. Michelangeli, P. A. Makar, D. R. Hastie, M. Mozurkewich and J. Auld, *Atmos*  
542 *Environ*, 2010, **44**, 361-369.
- 543 41. K. Sato, S. Hatakeyama and T. Imamura, *J Phys Chem A*, 2007, **111**, 9796-9808.
- 544 42. J. H. Kroll, N. L. Ng, S. M. Murphy, R. C. Flagan and J. H. Seinfeld, *Geophys Res Lett*, 2005, **32**,  
545 L18808.
- 546 43. N. L. Ng, J. H. Kroll, A. W. H. Chan, P. S. Chhabra, R. C. Flagan and J. H. Seinfeld, *Atmos Chem Phys*,  
547 2007, **7**, 3909-3922.
- 548 44. J. Liu, P. Lin, J. Laskin, A. Laskin and J. E. Shilling, *to be submitted to Atmospheric Chemistry and*  
549 *Physics*, 2015.
- 550 45. A. Hecobian, X. Zhang, M. Zheng, N. Frank, E. S. Edgerton and R. J. Weber, *Atmos Chem Phys*,  
551 2010, **10**, 5965-5977.
- 552 46. J. Liu, M. Bergin, H. Guo, L. King, N. Kotra, E. Edgerton and R. J. Weber, *Atmos Chem Phys*, 2013,  
553 **13**, 12389-12404.
- 554 47. P. J. Roach, J. Laskin and A. Laskin, *Analyst*, 2010, **135**, 2233-2236.
- 555 48. P. J. Roach, J. Laskin and A. Laskin, *Anal Chem*, 2010, **82**, 7979-7986.
- 556 49. N. Jaitly, A. Mayampurath, K. Littlefield, J. N. Adkins, G. A. Anderson and R. D. Smith, *Bmc*  
557 *Bioinformatics*, 2009, **10**, 87.
- 558 50. P. A. Eckert, P. J. Roach, A. Laskin and J. Laskin, *Anal Chem*, 2012, **84**, 1517-1525.
- 559 51. P. J. Roach, J. Laskin and A. Laskin, *Anal Chem*, 2011, **83**, 4924-4929.
- 560 52. M. J. Frisch, G. W. Trucks, H. B. Schlegel, G. E. Scuseria, M. A. Robb, J. R. Cheeseman, V. G.  
561 Zakrzewski, J. A. Montgomery Jr., R. E. Stratmann, J. C. Burant, S. Dapprich, J. M. Millam, A. D.  
562 Daniels, K. N. Kudin, M. C. Strain, O. Farkas, J. Tomasi, V. Barone, M. Cossi, R. Cammi, B.  
563 Mennucci, C. Pomelli, C. Adamo, S. Clifford, J. Ochterski, G. A. Petersson, P. Y. Ayala, Q. Cui, K.  
564 Morokuma, P. Salvador, J. J. Dannenberg, D. K. Malick, A. D. Rabuck, K. Raghavachari, J. B.  
565 Foresman, J. Cioslowski, J. V. Ortiz, A. G. Baboul, B. B. Stefanov, G. Liu, A. Liashenko, P. Piskorz, I.  
566 Komaromi, R. Gomperts, R. L. Martin, D. J. Fox, T. Keith, M. A. Al-Laham, C. Y. Peng, A.  
567 Nanayakkara, M. Challacombe, P. M. W. Gill, B. Johnson, W. Chen, M. W. Wong, J. L. Andres, C.  
568 Gonzalez, M. Head-Gordon, E. S. Replogle and J. A. Pople, *Gaussian 98* (2002) Gaussian, Inc.,  
569 Pittsburgh, PA.
- 570 53. R. Bauernschmitt and R. Ahlrichs, *Chem Phys Lett*, 1996, **256**, 454-464.
- 571 54. K. Hirayama, *Handbook of Ultraviolet and Visible Absorption Spectra of Organic Compounds*,  
572 Plenum Press Data Division, New York, 1967.

- 573 55. D. Hu, M. Tolocka, Q. Li and R. M. Kamens, *Atmos Environ*, 2007, **41**, 6478-6496.
- 574 56. J. F. Hamilton, P. J. Webb, A. C. Lewis and M. M. Reviejo, *Atmos Environ*, 2005, **39**, 7263-7275.
- 575 57. R. Koch, R. Knispel, M. Elend, M. Siese and C. Zetzsch, *Atmos Chem Phys*, 2007, **7**, 2057-2071.
- 576 58. R. Knispel, R. Koch, M. Siese and C. Zetzsch, *Ber Bunsen Phys Chem*, 1990, **94**, 1375-1379.
- 577 59. M. Kalberer, D. Paulsen, M. Sax, M. Steinbacher, J. Dommen, A. S. H. Prevot, R. Fisseha, E. Weingartner, V. Frankevich, R. Zenobi and U. Baltensperger, *Science*, 2004, **303**, 1659-1662.
- 579 60. M. S. Jang, N. M. Czoschke, S. Lee and R. M. Kamens, *Science*, 2002, **298**, 814-817.
- 580 61. D. Johnson, M. E. Jenkin, K. Wirtz and M. Martin-Reviejo, *Environ Chem*, 2004, **1**, 150-165.
- 581 62. H.-H. Perkampus, *UV-Vis Atlas of Organic Compounds*, Weinheim, New York, 1992.
- 582 63. V. V. Lobodin, A. G. Marshall and C. S. Hsu, *Anal Chem*, 2012, **84**, 3410-3416.
- 583 64. A. W. Birdsall, J. F. Andreoni and M. J. Elrod, *J Phys Chem A*, 2010, **114**, 10655-10663.
- 584 65. J. A. Dean, *Lange's Handbook of Chemistry*, McGraw-Hill, New York, 1992.
- 585 66. J. P. Cornard, Rasmiwetti and J. C. Merlin, *Chem Phys*, 2005, **309**, 239-249.
- 586 67. D. Prakash, J. Pandey, B. N. Tiwary and R. K. Jain, *Bmc Biotechnol*, 2010, **10**, 49.
- 587 68. K. Sato, A. Takami, Y. Kato, T. Seta, Y. Fujitani, T. Hikida, A. Shimono and T. Imamura, *Atmos Chem Phys*, 2012, **12**, 4667-4682.
- 589 69. A. W. H. Chan, G. Isaacman, K. R. Wilson, D. R. Worton, C. R. Ruehl, T. Nah, D. R. Gentner, T. R. Dallmann, T. W. Kirchstetter, R. A. Harley, J. B. Gilman, W. C. Kuster, J. A. deGouw, J. H. Offenberg, T. E. Kleindienst, Y. H. Lin, C. L. Rubitschun, J. D. Surratt, P. L. Hayes, J. L. Jimenez and A. H. Goldstein, *J Geophys Res-Atmos*, 2013, **118**, 6783-6796.
- 593 70. J. J. Schauer, M. J. Kleeman, G. R. Cass and B. R. T. Simoneit, *Environ Sci Technol*, 1999, **33**, 1578-1587.
- 595 71. M. A. Gough and S. J. Rowland, *Nature*, 1990, **344**, 648-650.
- 596 72. D. R. Stoll, X. P. Li, X. O. Wang, P. W. Carr, S. E. G. Porter and S. C. Rutan, *J Chromatogr A*, 2007, **1168**, 3-43.
- 598 73. L. Ran, C. S. Zhao, W. Y. Xu, M. Han, X. Q. Lu, S. Q. Han, W. L. Lin, X. B. Xu, W. Gao, Q. Yu, F. H. Geng, N. Ma, Z. Z. Deng and J. Chen, *Atmos Chem Phys*, 2012, **12**, 7531-7542.
- 600 74. E. Bolzacchini, M. Bruschi, J. Hjorth, S. Meinardi, M. Orlandi, B. Rindone and E. Rosenbohm, *Environ Sci Technol*, 2001, **35**, 1791-1797.
- 602 75. D. Vione, V. Maurino, C. Minero, M. Lucchiari and E. Pelizzetti, *Chemosphere*, 2004, **56**, 1049-1059.
- 604 76. J. Tremp, P. Mattrel, S. Fingler and W. Giger, *Water Air Soil Poll*, 1993, **68**, 113-123.
- 605 77. Y. Iinuma, O. Boge, R. Grafe and H. Herrmann, *Environ Sci Technol*, 2010, **44**, 8453-8459.
- 606 78. J. Ehlerova, L. Trevani, J. Sedlbauer and P. Tremaine, *J Solution Chem*, 2008, **37**, 857-874.
- 607 79. M. Roses, F. Rived and E. Bosch, *J Chromatogr A*, 2000, **867**, 45-56.
- 608 80. K. B. Budhavant, P. S. P. Rao, P. D. Safai, L. Granat and H. Rodhe, *Atmos Environ*, 2014, **88**, 59-65.
- 609 81. Y. Wang, J. Guo, T. Wang, A. J. Ding, J. A. Gao, Y. Zhou, J. L. Collett and W. X. Wang, *Atmos Res*, 2011, **99**, 434-442.
- 611 82. S. L. Clegg, P. Brimblecombe and A. S. Wexler, *J Phys Chem A*, 1998, **102**, 2137-2154.
- 612 83. A. Nenes, S. N. Pandis and C. Pilinis, *Aquat Geochem*, 1998, **4**, 123-152.
- 613 84. K. He, Q. Zhao, Y. Ma, F. Duan, F. Yang, Z. Shi and G. Chen, *Atmos Chem Phys*, 2012, **12**, 1377-1395.
- 615 85. Z. Y. Meng, J. H. Seinfeld, P. Saxena and Y. P. Kim, *Aerosol Sci Tech*, 1995, **22**, 111-123.
- 616 86. J. Xue, A. K. H. Lau and J. Z. Yu, *Atmos Environ*, 2011, **45**, 7081-7088.
- 617 87. S. Fujita, A. Takahashi, J. H. Weng, L. F. Huang, H. K. Kim, C. K. Li, F. T. C. Huang and F. T. Jeng, *Atmos Environ*, 2000, **34**, 525-537.
- 619 88. A. H. Tang, G. S. Zhuang, Y. Wang, H. Yuan and Y. L. Sun, *Atmos Environ*, 2005, **39**, 3397-3406.
- 620 89. S. Ghorai, B. B. Wang, A. Tivanski and A. Laskin, *Environ Sci Technol*, 2014, **48**, 2234-2241.

- 621 90. A. Laskin, R. C. Moffet, M. K. Gilles, J. D. Fast, R. A. Zaveri, B. B. Wang, P. Nigge and J.  
622 Shutthanandan, *J Geophys Res-Atmos*, 2012, **117**, D15302.  
623 91. B. B. Wang and A. Laskin, *J Geophys Res-Atmos*, 2014, **119**, 3335-3351.  
624

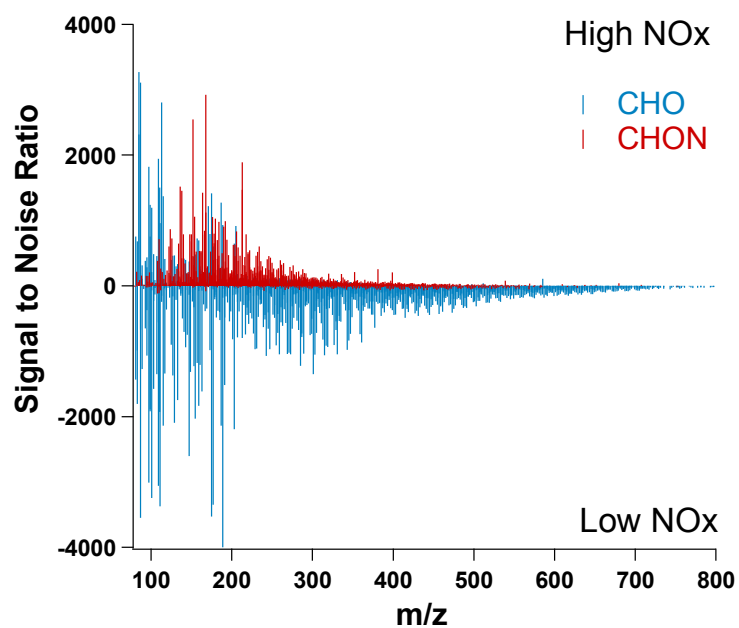
Tables and Figures

Figure 1:



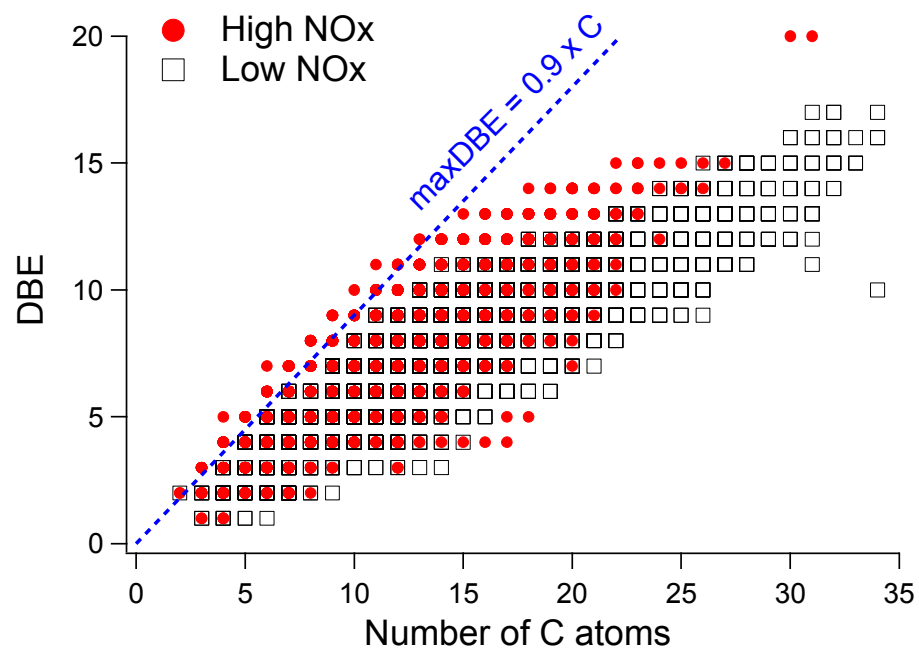
**Figure 1.** Photographs of the Tol-SOA samples collected in toluene photooxidation experiments performed under high-NO<sub>x</sub> and low-NO<sub>x</sub> conditions, indicating distinct optical properties of Tol-SOA produced under different initial NO<sub>x</sub> concentrations. The plot on the right compares their mass absorption coefficients ( $\text{MAC}_{\text{bulk}}$ ) in wavelength range 300-700 nm.

Figure 2:



**Figure 2.** Negative mode nano-DESI/HRMS spectra of Tol-SOA samples generated under high-NOx (positive intensities) and low-NOx conditions (negative intensities). Formulas are grouped based on their elemental composition (see text for details).

Figure 3:



**Figure 3.** Plot of double bond equivalent (DBE) values as a function of the number of carbon atoms for molecules identified in Tol-SOA produced under high NO<sub>x</sub> (red dots) and low-NO<sub>x</sub> conditions (black squares). The blue dashed line indicates the upper compositional boundary for naturally occurring hydrocarbons in fossil resources.<sup>63</sup>

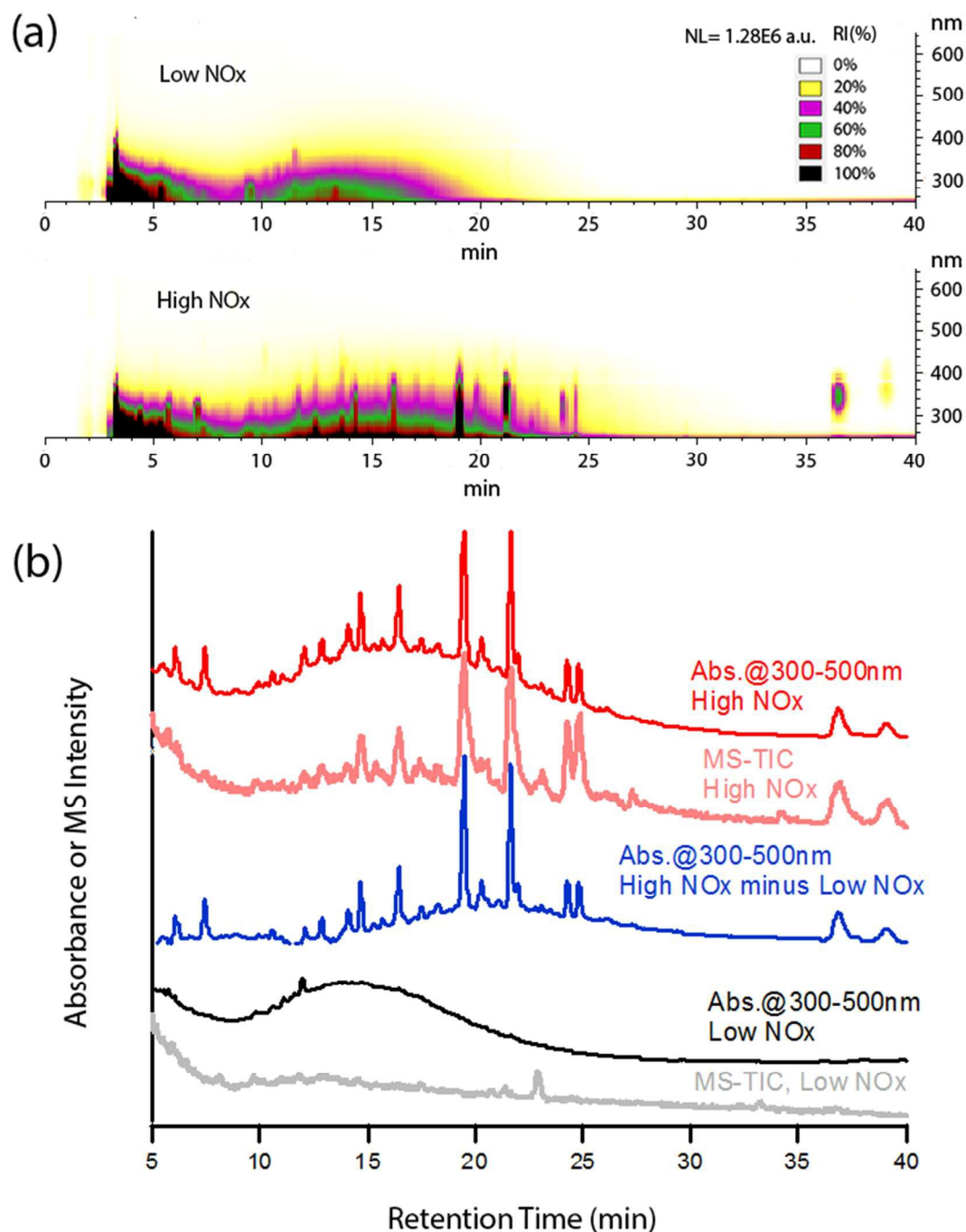


**Figure 4.** (a) The plot of PDA signals as a function of retention time (min) and light wavelength (nm) for the Tol-SOA sample produced under low-NO<sub>x</sub> and high-NO<sub>x</sub> conditions, respectively. (b) UV/Vis photodiode array (PDA) detector chromatogram and MS total ion count (TIC) chromatogram of Tol-SOA samples generated under high-NO<sub>x</sub> and low-NO<sub>x</sub> conditions. The absorbance signals were integrated over wavelengths of 300-500nm. The blue plot shows the difference of the PDA chromatograms between high-NO<sub>x</sub> (red) and low-NO<sub>x</sub> (black) chromatograms. The intensities are offset along y-axis to facilitate comparison.

Figure 5:

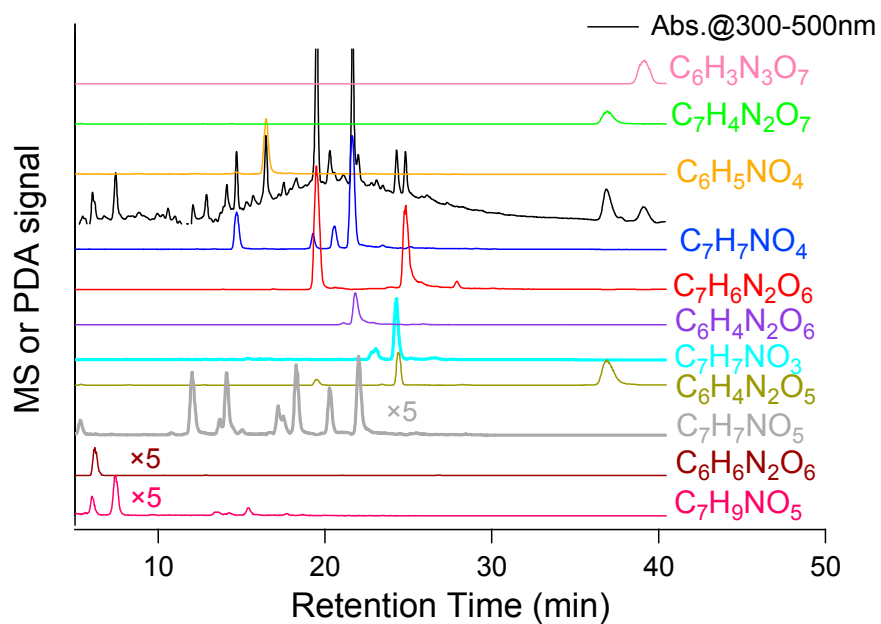
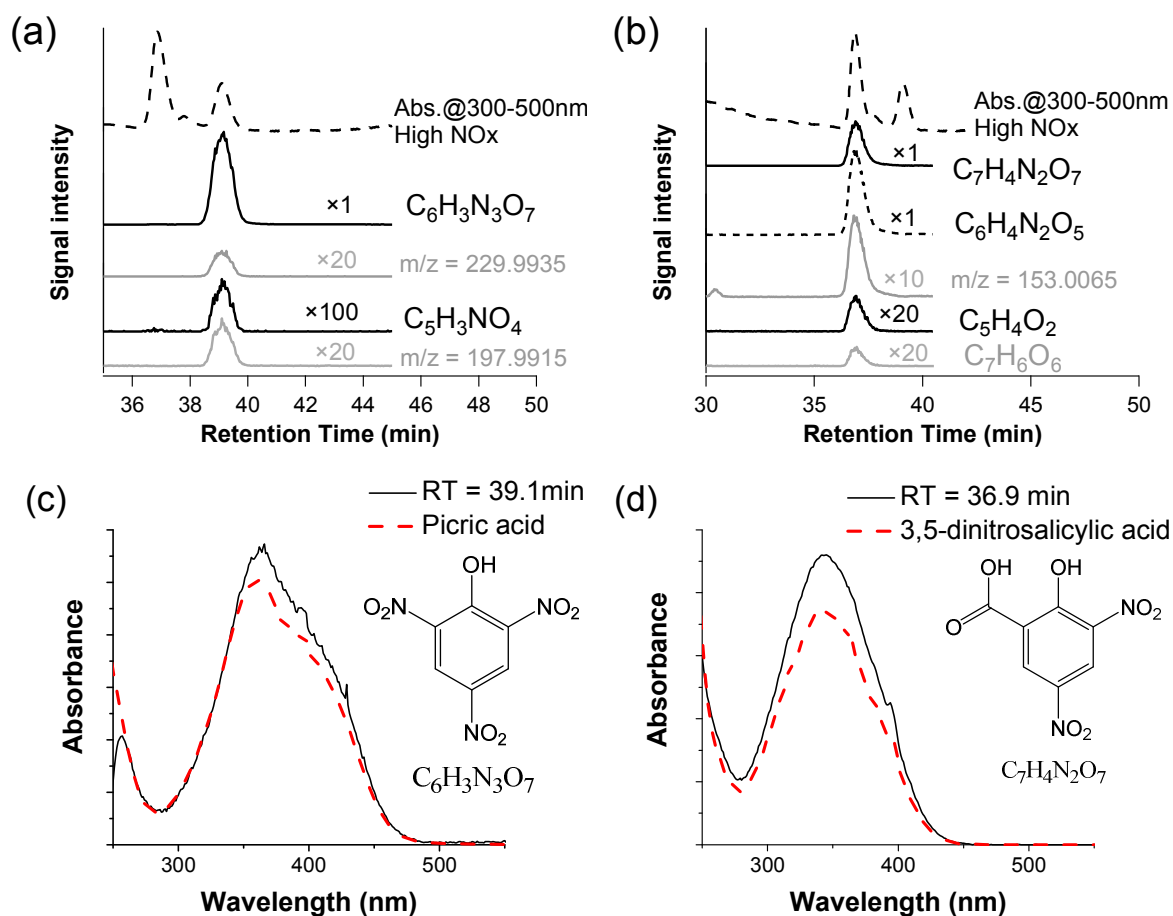


Figure 5. A UV/Vis (PDA) chromatogram integrated over 300-500nm (black trace) and MS extracted ion chromatograms (EIC) of major BrC chromophores observed in the sample of high-NO<sub>x</sub> Tol-SOA.

Figure 6:



**Figure 6.** Extracted ion chromatograms (EIC) of molecules co-eluted at (a) 39.1 min and (b) 36.9 min. Panel (c) compares the UV/Vis spectra of the BrC chromophore in high-NOx Tol-SOA sample eluting at 39.1 min with the spectrum of picric acid measured by PDA. Panel (d) compares the UV/Vis spectrum of the BrC chromophore in high-NOx Tol-SOA sample eluting at 36.9 min with the spectrum of 3,5-dinitrosalicylic acid measured by PDA.

Figure 7

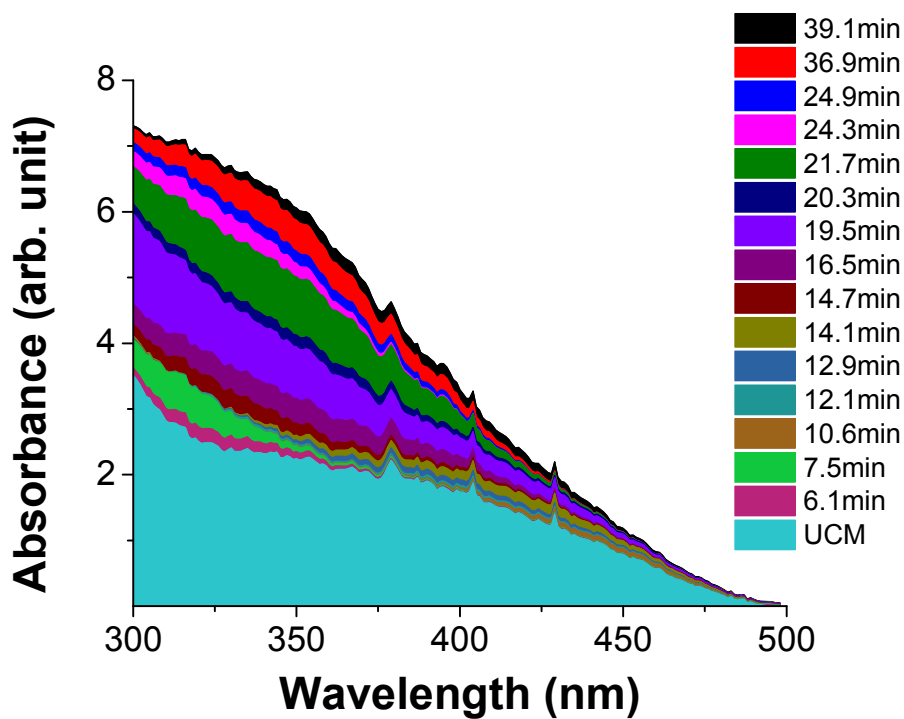
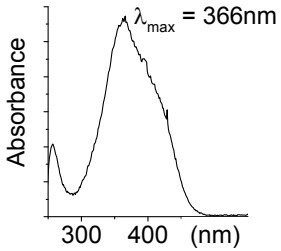
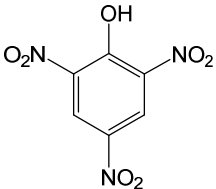
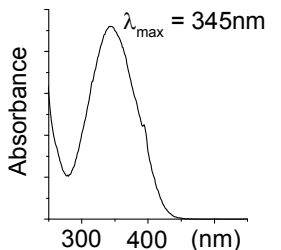
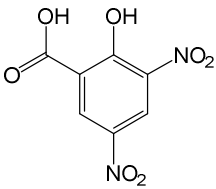
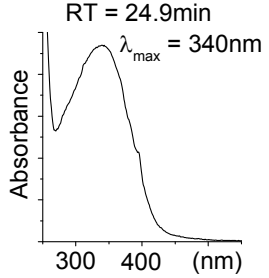
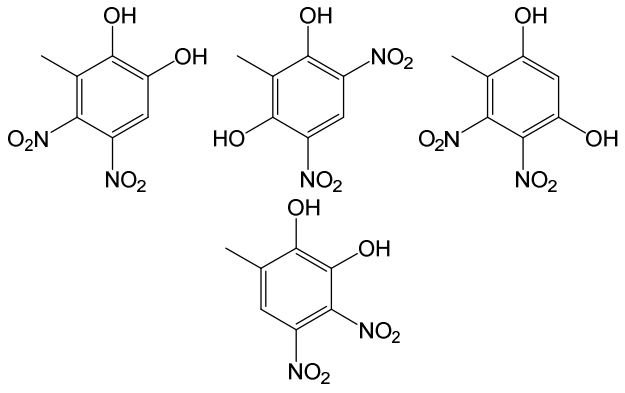
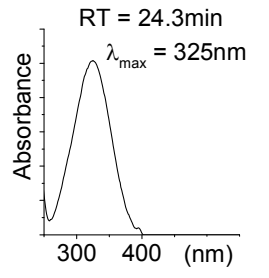
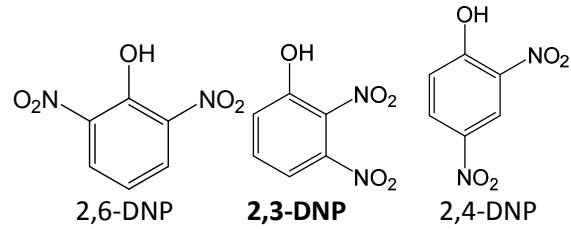
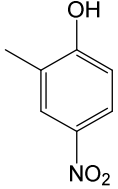
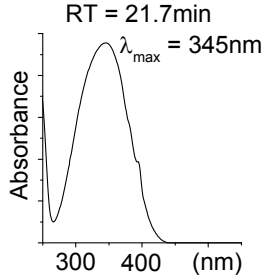
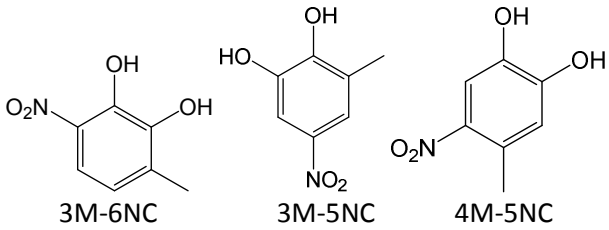
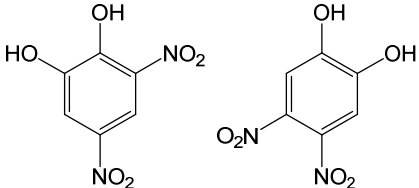


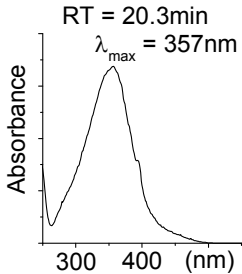
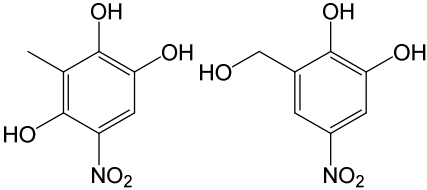
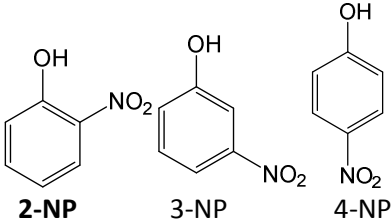
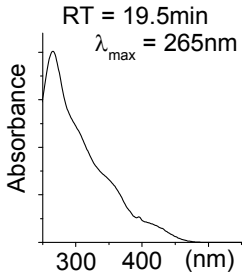
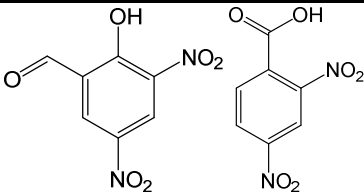
Figure 7. The relative contribution of the fifteen identified BrC chromophores and the unresolved complex mixtures (UCM, see text) with respect to the total light absorption by high-NO<sub>x</sub> Tol-SOA recorded in the HPLC-PDA measurement.

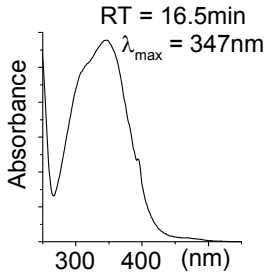
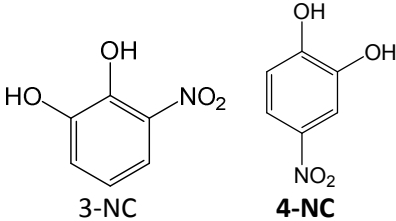
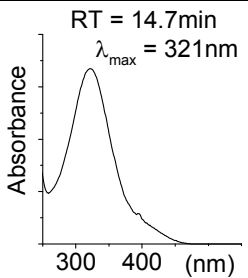
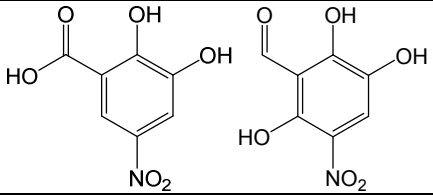
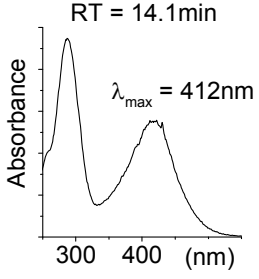
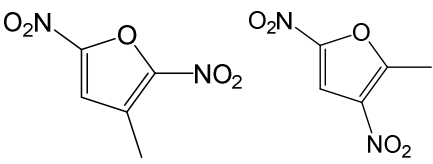
Table 1. Summary of the PDA spectra and retention times (RT) of major light-absorbing peaks and elemental formulas of the corresponding chromophoric compounds. The PDA spectra of some commercially available compounds or the maximum absorption wavelength ( $\lambda_{\max}$ ) of several organic compounds reported in the literature are also listed for comparison.

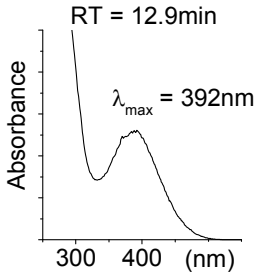
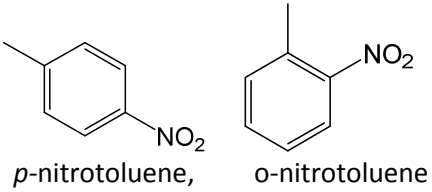
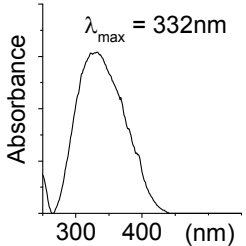
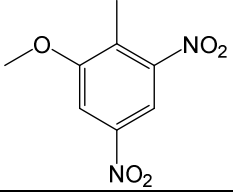
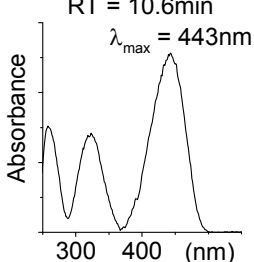
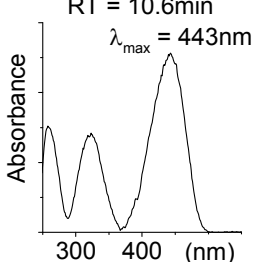
PDA spectrum @RT(min)	Formula and candidate compound	Proposed Structures	Comments
<p>RT = 39.1 min</p>  <p>Absorbance</p> <p>300 400 (nm)</p> <p><math>\lambda_{\max} = 366\text{nm}</math></p>	<p><math>\text{C}_6\text{H}_3\text{N}_3\text{O}_7</math>, picric acid</p>		<p>Identification of molecular structure was assisted by the analysis of commercially available standard of picric acid as shown in Figure 6a</p>
<p>RT = 36.9 min</p>  <p>Absorbance</p> <p>300 400 (nm)</p> <p><math>\lambda_{\max} = 345\text{nm}</math></p>	<p><math>\text{C}_7\text{H}_4\text{N}_2\text{O}_7</math>, 3,5-dinitrosalicylic acid</p>		<p>Identification of molecular structure was assisted by the analysis of commercially available standard of 3,5-dinitrosalicylic acid as shown in Figure 6b</p>

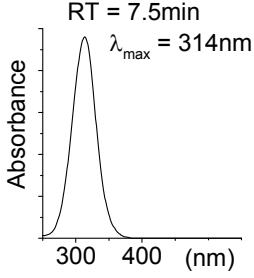
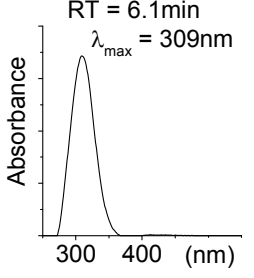
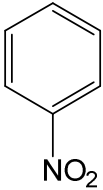
	<p>*  <math>C_7H_6N_2O_6</math>,  Methyl-  dinitrocatechol</p>		<p>Specific positions of <math>-NO_2</math> and <math>-OH</math> groups in different isomers influence their absorption characteristics. Molecular structures with <math>NO_2</math> groups in 1,4 (<i>para</i>) positions are likely to be most absorbing, followed by 1,3 (<i>ortho</i>) and 1,2 (<i>meta</i>) isomers. Positions of <math>-OH</math> are expected to have additional, but less pronounced effect. For details, see comments to the chromophore at <math>RT=21.7min</math>.</p>
	<p><math>C_6H_4N_2O_5</math>,  dinitrophenols (DNP)</p>		<p>Molecular structure of 2,3-dinitrophenol (2,3-DNP) is suggested as a plausible chromophore based on the literature report<sup>30</sup> of <math>\lambda_{max}=329nm</math> for 2,3-DNP, as opposed to <math>\lambda_{max}=350nm</math> for 2,6-DNP and <math>\lambda_{max}=292nm</math> for 2,4-DNP.</p>
	<p><math>C_7H_7NO_3</math>,  nitrocresols</p>		<p>Molecular structure of 4-nitro-<i>o</i>-cresol is suggested as a plausible chromophore based on the literature report of <math>\lambda_{max}=319nm</math><sup>30</sup></p>

	<p>** C<sub>7</sub>H<sub>7</sub>NO<sub>4</sub>, Methyl-nitrocatechol (M-NC)</p>		<p>Relative UV-Vis absorption of methyl-nitrocatechol (M-NC) and dinitrocatechol (DNC) isomers was evaluated using theoretical chemistry calculations of electronic structures for isolated molecules with the scope to assess effects of the functional groups positions (see Figure S2 for details). The results of these calculations are summarised below:</p> <ol style="list-style-type: none"> <li>1) Presence or absence of –CH<sub>3</sub> group and its specific position on the aromatic ring have no coherent impact on the UV-Vis absorption (see structures 1-3 of Fig S2)</li> <li>2) Specific positions of –OH and –NO<sub>2</sub> groups influence the UV-Vis absorption of M-NC isomers. Molecular structures with 1,2-OH 3-NO<sub>2</sub> and 1,4-OH 3-NO<sub>2</sub> groups are predicted to have enhanced absorption in the Vis region (see structures 3-7 of Fig S2).</li> </ol>
	<p>C<sub>6</sub>H<sub>4</sub>N<sub>2</sub>O<sub>6</sub>, Dinitrocatechol</p>		<ol style="list-style-type: none"> <li>2) Specific positions of –OH and –NO<sub>2</sub> groups influence the UV-Vis absorption of DNC isomers. Molecular structures with NO<sub>2</sub> groups in 1,4 (<i>para</i>) positions are</li> </ol>

			predicted to be the most absorbing, followed by 1,3 ( <i>ortho</i> ) and 1,2 ( <i>meta</i> ) isomers. Positions of –OH groups have additional but less pronounced influence. (see structures 8-14 of Fig S2).
	<p>*** C<sub>7</sub>H<sub>7</sub>NO<sub>5</sub></p>		
	<p>C<sub>6</sub>H<sub>5</sub>NO<sub>3</sub>, Nitrophenol</p>		<p>Molecular structure of 2-Nitrophenol (2-NP) is suggested as a plausible chromophore based on the literature report of <math>\lambda_{\text{max}}=351\text{nm}</math> for 2-NP, as opposed to <math>\lambda_{\text{max}}=333\text{nm}</math> for 3-NP and <math>\lambda_{\text{max}}=317\text{nm}</math> for 4-NP.<sup>30</sup></p>
	<p>** C<sub>7</sub>H<sub>7</sub>NO<sub>4</sub>, Methyl-nitrocatechol</p>		<p>** see comments to the chromophore at RT=21.7min.</p>
	<p>C<sub>7</sub>H<sub>4</sub>N<sub>2</sub>O<sub>6</sub>,</p>		
	<p>* C<sub>7</sub>H<sub>6</sub>N<sub>2</sub>O<sub>6</sub>, Methyl-dinitrocatechol</p>		<p>* see comments to the chromophore at RT=24.9min.</p>

	** C <sub>7</sub> H <sub>7</sub> NO <sub>4</sub> , Methyl-nitrocatechol		** see comments to the chromophore at RT=21.7min.
	C <sub>6</sub> H <sub>5</sub> NO <sub>4</sub> , Nitrocatechol		Molecular structure of 4-Nitrocatechol (4-NC) is suggested as a plausible chromophore based on the literature report of $\lambda_{\max}=345\text{nm}^{66}$ for 4-NC, as opposed to $\lambda_{\max}=296\text{nm}$ for 3-NC.
	C <sub>7</sub> H <sub>5</sub> NO <sub>6</sub>		
	** C <sub>7</sub> H <sub>7</sub> NO <sub>4</sub> , Methyl-nitrocatechol		** see comments to the chromophore at RT=21.7min.
	C <sub>5</sub> H <sub>4</sub> N <sub>2</sub> O <sub>5</sub> ;		
	*** C <sub>7</sub> H <sub>7</sub> NO <sub>5</sub>		

 <p>RT = 12.9min <math>\lambda_{\max} = 392\text{nm}</math></p>	<p><math>\text{C}_7\text{H}_7\text{NO}_2</math>, nitro-toluene</p>	 <p><i>p</i>-nitrotoluene,    <i>o</i>-nitrotoluene</p>	<p>These two compounds have <math>\lambda_{\max}</math> around 260nm, with a broad shoulder from 300nm to 400nm. (NIST Standard Reference Database Number 69, <a href="http://webbook.nist.gov">http://webbook.nist.gov</a>)</p>
 <p>RT = 12.1min <math>\lambda_{\max} = 332\text{nm}</math></p>	<p><math>\text{C}_8\text{H}_8\text{N}_2\text{O}_5</math></p>		
 <p>RT = 10.6min <math>\lambda_{\max} = 443\text{nm}</math></p>	<p><math>\text{C}_7\text{H}_9\text{NO}_5</math> DBE=4</p>		<p>Based on the low DBE value, corresponding molecular structure is likely non-aromatic</p>
 <p>RT = 10.6min <math>\lambda_{\max} = 443\text{nm}</math></p>	<p><math>\text{C}_7\text{H}_8\text{N}_2\text{O}_7</math> DBE=5</p>		<p>Based on the low DBE value, corresponding molecular structure is likely non-aromatic</p>
	<p><math>\text{C}_8\text{H}_{13}\text{NO}_8</math> DBE=3</p>		<p>Based on the low DBE value, corresponding molecular structure is likely non-aromatic</p>

 <p>RT = 7.5min <math>\lambda_{\max} = 314\text{nm}</math></p>	<p><math>\text{C}_7\text{H}_9\text{NO}_5</math> DBE=4</p>		<p>Based on the low DBE value, corresponding molecular structure is likely non-aromatic</p>
 <p>RT = 6.1min <math>\lambda_{\max} = 309\text{nm}</math></p>	<p><math>\text{C}_6\text{H}_5\text{NO}_2</math> Nitrobenzene</p>		<p>Molecular structure of nitrobenzene (NB) is suggested as plausible chromophore. (<math>\lambda_{\max}=280\text{nm}</math> has been reported<sup>30</sup> for NB).</p>
	<p><math>\text{C}_6\text{H}_6\text{N}_2\text{O}_6</math> DBE=5</p>		

\* potential chromophores with the same elemental formula ( $\text{C}_7\text{H}_6\text{N}_2\text{O}_6$ ) appear at RT= 24.9 and 19.5min

\*\* potential chromophores with the same elemental formula ( $\text{C}_7\text{H}_7\text{NO}_4$ ) appear at RT= 21.7, 20.3, 19.5 and 14.7 min

\*\*\* potential chromophores with the same elemental formula ( $\text{C}_7\text{H}_7\text{NO}_5$ ) appear at RT= 20.3, 14.1 min

Table 2. The acid dissociation constants (pKa) and maximum absorption wavelength of several nitro-phenolic compounds. (<sup>m</sup>the value is measured in this study for commercially available compounds. Other values are from literature reports)

Compound	pKa	$\lambda_p$ (nm) of neutral molecule	$\lambda_p$ (nm) of deprotonated molecule
2-nitrophenol	7.2 <sup>78</sup>	350	430
3-nitrophenol	8.4 <sup>78</sup>	330	420
4-nitrophenol	7.1 <sup>78</sup>	315	425
4-nitrocatechol	6.7 <sup>66</sup>	345	426
2,4-dinitrophenol	4.1 <sup>79</sup>	292 <sup>m</sup>	405 <sup>m</sup>
2,5-dinitrophenol	5.2 <sup>79</sup>	360 <sup>m</sup>	450 <sup>m</sup>
3,5-dinitrosalicylic acid	3.0	345 <sup>m</sup>	360 <sup>m</sup>
picric acid	0.3	360 <sup>m</sup>	390 <sup>m</sup>